Global and Planetary Change 220 (2023) 104025

Contents lists available at ScienceDirect

Global and Planetary Change

journal homepage: www.elsevier.com/locate/gloplacha

Variation in organic matter across the Cretaceous-Paleogene boundary in New Zealand supports the "Living Ocean" model of biotic recovery

Claudia Sosa-Montes de Oca [a,*], Kyle W.R. Taylor [b], Christopher J. Hollis [c], Yizhou Huang [a], Richard D. Pancost [a]

[a] Organic Geochemistry Unit, The Cabot Institute for the Environment, School of Earth Sciences, School of Chemistry, University of Bristol, BS8 1TS, UK
[b] Elementar UK Limited, Isoprime House, Earl Road, Cheadle Hulme, Cheadle SK8 6PT, UK
[c] School of Geography, Environment and Earth Sciences, Victoria University of Wellington, New Zealand

ARTICLE INFO

Editor: Fabienne Marret-Davies

Keywords:
Cretaceous-Paleogene boundary
Mid-Waipara River section
Biomarkers
Organic matter sources, reworked organic matter

ABSTRACT

The Cretaceous-Paleogene (K-Pg) boundary represents the most recent mass extinction in Earth history. Although it is widely accepted that a bolide impact in North America caused the extinction, many questions persist about how this impact affected Earth's climate and environment. Here we explore changes in organic matter inputs across the K-Pg in an impact-distal section in New Zealand (mid-Waipara River section, North Canterbury, New Zealand). The section is 21.2 m thick, including 1.2 m of uppermost Cretaceous and 20 m of lower Paleocene sediment, the latter spanning ~1 Myr, albeit interrupted by at least one major unconformity. We examine the abundance and distribution of *n*-alkanes and *n*-alkanoic acids (mixed sources), acyclic isoprenoids (pristane and phytane), steranes (eukaryotes), hopanes and hopanoic acids (bacteria) and GDGTs (glycerol dialkyl glycerol tetraether lipids) to explore changes in the relative contribution of marine vs terrestrial sources. Minimal differences in the biomarker assemblages between sediments below and above the K-Pg boundary suggest a rapid recovery of the non-fossilizing phytoplankton community, similar to that observed in other distal settings. However, the organic matter source became variable immediately after the impact event. Variations in the concentrations and distribution of the high-molecular-weight *n*-alkanes and *n*-alkanoic acids, terrestrial-aquatic ratios, and GDGT branched to isoprenoidal tetraether indices indicate an increase in the absolute and proportional abundance of terrestrial soil- and plant-derived organic matter just after the impact event. This co-occurs with an apparently transient decline in marine productivity, indicated by a decrease in concentrations of low-molecular-weight *n*-alkanoic acids, concentrations of pristane + phytane (of putative algal chlorophyll origin), and sterane/hopane ratios. This suggests that the bolide did affect the mid-Waipara biomarker-producing bacterial and algal assemblages, distinct from what has been observed at other distal sites. However, it remains unclear if this was a direct consequence of the impact or the wider post-impact reorganisation of environment and oceanography as has been previously observed in this region.

1. Introduction

The Cretaceous-Paleogene (K-Pg) boundary represents one of the five largest mass extinction events in Earth history and is also associated with major changes in the global environment (D'Hondt, 2005). The primary cause of the mass extinction event is inferred to be an asteroid impact (Hull et al., 2020; Pälike, 2013; Schulte et al., 2010). The role of additional factors, such as volcanism, is still being considered and debated (Gilabert et al., 2021; Renne et al., 2015; Schoene et al., 2019, 2015). After decades of research, there also remain critical questions about the nature and timing of biotic recovery from the K-Pg extinction (Bralower et al., 2020; Gulick et al., 2019; Lowery et al., 2020, 2018; Rodríguez-Tovar et al., 2020; Schaefer et al., 2020; Sepúlveda et al., 2019; Sosa-Montes de Oca et al., 2013, 2021, 2020, 2018). There are numerous outcrops worldwide where the K-Pg boundary has been recorded (e.g. Schulte et al., 2010), but the characteristics of each section differ depending on the distance from the Chicxulub crater (very proximal, proximal, intermediate and distal). The distal marine deposits, located >5000 km distance from the Chicxulub impact site and not affected by the immediate destructive forces of the impact (Kring, 2007),

* Corresponding authors.
E-mail address: claudia.sosamontesdeoca@bristol.ac.uk (C. Sosa-Montes de Oca).

https://doi.org/10.1016/j.gloplacha.2022.104025
Received 24 June 2022; Received in revised form 21 December 2022; Accepted 23 December 2022
Available online 26 December 2022

are particularly important for assessing global environmental consequences of the K-Pg event and biotic recovery after it.

In the marine realm, the K-Pg mass extinction is associated with a collapse in the carbon isotopic ($\delta^{13}C$) gradient between surface and seafloor carbonate $\delta^{13}C$ values. These perturbations have been explained by several hypotheses: the Strangelove Ocean hypothesis posits that primary productivity sharply decreased or ceased immediately after the K-Pg boundary due to the extinction of primary producers (Hsü et al., 1982; Hsü and McKenzie, 1985; Keller and Lindinger, 1989; Stott and Kennett, 1989; Zachos et al., 1992, 1989); the Living Ocean hypothesis postulates that marine primary productivity did not decrease but export productivity (total organic carbon that sank to the deep ocean via the biological pump) was dramatically reduced for a few hundred thousand years and moderately reduced for millions of years after K-Pg mass extinction (Adams, 2004; Birch et al., 2016; Coxall et al., 2006; D'Hondt, 2005; D'Hondt et al., 1998); or recently, the Heterogeneous Ocean hypothesis proposes a geographic heterogeneity in the change of export productivity in the wake of the K-Pg mass extinction (Esmeray-Senlet et al., 2015). In contrast, terrestrial ecosystems are believed to have recovered more quickly from the K-Pg event than counterpart marine ecosystems (Beerling et al., 2001). A shutdown or reduction in the uptake of ^{12}C by photosynthetic phytoplankton and increased biomass burning (Ivany and Salawitch, 1993; Lyons et al., 2020; Wolbach et al., 1988) could together have led to elevated levels of CO_2 in the atmospheric reservoir (Milligan et al., 2022). Evidence for the transfer of CO_2 from the atmosphere to the terrestrial biosphere reservoir (via photosynthesis) is reflected in a negative carbon isotope excursion (CIE) recorded in $\delta^{13}C$ of terrestrial biomarkers in Europe (Arinobu et al., 1999; Sepúlveda et al., 2019) and bulk terrestrial organic matter from sites in North America (Arens and Jahren, 2000; Schimmelmann and DeNiro, 1984).

Biomarkers preserved in sedimentary sequences and structurally linked to specific biological sources (e.g. Eglinton and Eglinton, 2008; Peters et al., 2005) are powerful tools for exploring biotic changes and organic matter (OM) sources (Xie et al., 2010). Moreover, biomarker degradation and alteration is governed by environmental conditions, such that they can be also used to reconstruct palaeoenvironmental conditions (e.g. Eglinton and Eglinton, 2008; Peters et al., 2005). However, applications of biomarkers to explore post K-Pg changes in biotic assemblages in distal sections are limited, as are their application to understanding changes in organic matter source and the expression of organic $\delta^{13}C$ records. Sepúlveda et al. (2009) used sterane distributions to argue for blooms of algae just above the boundary in the Fish Clay of Denmark (Stevns Klint distal section), and then a rapid recovery to pre-event distributions. Sosa-Montes de Oca et al. (2021) used the distribution of specific phytoplankton (pristane, phytane, steranes), vascular plant (*n*-alkanes) and bacterial (hopanes) biomarkers at the Agost distal section (Spain) to reveal highly variable terrigenous inputs immediately preceding and right after K-Pg boundary but minimal changes in the algal and bacterial assemblages. Similarly, Bralower et al. (2020) analysed the micrite-rich layer (boundary clay) at 31 sites across the world, to argue for transient ocean-wide blooms of cyanobacteria and algae in the millennia after the K-Pg boundary impact event. However, biotic and environmental responses are likely to be highly variable in different settings, and obtaining further records is critical to understanding post-impact biotic recovery.

The mid-Waipara River section (MW), North Canterbury (New Zealand) is the most complete known record of the K-Pg boundary from a neritic setting in the South Pacific region (Brooks et al., 1986; Hollis and Strong, 2003; Strong, 1984), providing a crucial link between bathyal marine and terrestrial records. The presence of sufficiently abundant and thermally immature organic carbon (Taylor et al., 2018) makes the section ideal for organic geochemical analysis. Here, we present analysis through a 21.2 m interval of the mid-Waipara River section. We examine the abundance and distribution of *n*-alkanes and *n*-alkanoic acids (mixed sources), acyclic isoprenoids (pristane [Pr] and phytane [Ph]), steranes (eukaryotes), hopanes and hopanoic acids (bacteria) and glycerol dialkyl glycerol tetraether lipids (GDGTs). Crucially, the presence of terrestrially derived biomarkers (i.e., high-molecular-weight *n*-alkanes and *n*-alkanoic acids) allows us to explore, for first time in this marine section, changes in the relative contribution of marine vs terrestrial sources. These analyses also allow us to interpret the bulk organic matter carbon isotopic profile across the event, which we further interrogate using the carbon isotopic composition of specific biomarkers. This allows us to explore how the carbon cycle was perturbed and subsequently recovered in terrestrial and marine systems across the K-Pg boundary and into the early Danian.

2. Geological setting

Latest Cretaceous sediments in the mid-Waipara River (MW) section (Fig. 1) are inferred to have been deposited in a middle to outer shelf setting (~200 m) within a neritic water mass (Hollis and Strong, 2003) at ~55° S palaeolatitude (Hollis, 2003) and located ~10,500 km from the Chicxulub impact site (Schulte et al., 2010). The section is located on a bank on the right side of the Waipara River c. 1 km upstream from the Laidmore Station road crossing (Hollis and Strong, 2003). Lithologically, the upper Maastrichtian (uppermost Cretaceous) comprises muddy calcareous glauconitic sandstone and is included in the Conway Formation. The lower Danian (Paleogene) consists of 4-m thick, largely non-calcareous, glauconitic sandstone which forms the uppermost unit of the Conway Formation, overlain by 16 m of the Loburn Formation, a non-calcareous to slightly calcareous siltstone. Geochemical studies place the K-Pg boundary at the base of an irregular 2-cm thick, 'rusty' Fe-stained interval that includes a relatively small Ir anomaly (0.49 ng g^{-1}, ~50 × crustal average) as well as enrichment in Fe, Ni, Zn and Cr. These elemental anomalies suggest that bioturbation affected 5 cm above and below K-Pg boundary. The boundary also coincides with a marked decrease in $CaCO_3$ concentration from ~30 wt% in the Cretaceous to <5 wt% over the lower 5 m of Paleocene strata (Hollis and Strong, 2003). A second "rusty" zone 21.5 cm above the K-Pg boundary is also associated with Fe and Cr enrichments and is inferred to represent an unconformity of ~1 myr (Taylor et al., 2018). The combined enrichment of these elements over an extended interval may indicate dysoxic conditions (Calvert and Pedersen, 1993).

The 21.2 m-thick K-Pg interval studied is considered to span a time interval of ~1.9 myr, ranging from ~0.2 myr before to ~1.7 myr after the K-Pg boundary (Taylor et al., 2018). The age model of Taylor et al. (2018) indicates that the compacted sedimentation rate was 9.4 m myr^{-1} for the 1.2 m of uppermost Maastrichtian sediments; 5.7 m myr^{-1} for the first 0.215 m above K-Pg boundary, 14.6 m myr^{-1} from 0.215 to 7.84 m above K-Pg boundary and 44.3 m myr^{-1} from 7.84 to 20.00 m. Within this stratigraphic context, the ejecta layer deposition itself was a snapshot on the geological time scale, potentially, on the order of days to months (Artemieva and Morgan, 2009), but it is not discreetly preserved.

3. Methods

3.1. Total Organic Carbon (TOC)

TOC, and biomarker analyses were performed on 26 samples distributed along the 21.2 m section, with higher resolution closer to the K-Pg boundary. TOC concentration was determined (Taylor et al., 2018) by subtracting the inorganic carbon (IC) from the total carbon (TC) content in each sample, both determined with a SHIMADZU TOC-VCSH.

3.2. Biomarker analyses

For biomarker analyses, 10 to 32 g of sediment were freeze-dried, powdered and extracted via Soxhlet apparatus for 24 h using dichloromethane (DCM)/methanol (MeOH) (2:1 *v*/v) following the method of

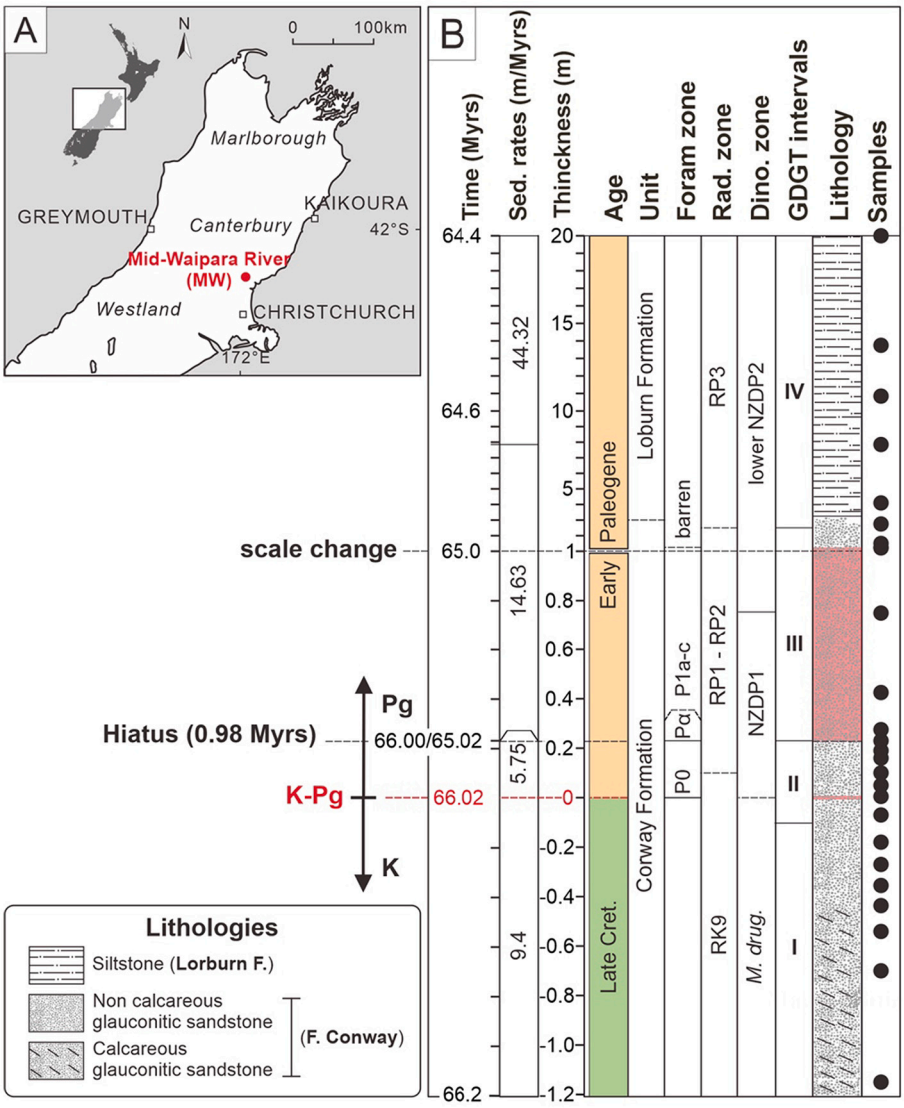

Fig. 1. Location and chronostratigraphy of the mid-Waipara K-Pg section [modified by Taylor et al., 2018]. (A) Location of the Cretaceous-Paleogene (K-Pg) section at the mid-Waipara River outcrop (Canterbury, East of New Zealand). (B) Stratigraphy profile for the uppermost Cretaceous and lower Paleogene succession at the mid-Waipara River section comprised by: uppermost Maastrichtian mud-rich and calcareous glauconitic from the, while lower Danian consisted in 4 m thick, non-calcareous glauconitic sandstone, which forms the uppermost unit of the Conway Formation, overlain by 15 m of a non-calcareous to slightly calcareous siltstone from the Loburn Formation.

Taylor et al. (2013). The total lipid extracts (TLE) were separated into two fractions on an aminopropyl solid phase extraction column by elution with DCM/isopropanol (2:1 v/v; neutral fraction) and 2% acetic acid in diethyl ether (acid fraction). The neutral fraction was further split using a column packed with activated alumina by elution with hexane/DCM (9:1 v/v; apolar fraction) and DCM/MeOH (1:2 v/v; polar fraction), and all fractions were evaporated to dryness under a steady flow of nitrogen. The neutral apolar fraction and acid fraction were analysed by gas chromatography–mass spectrometry (GC–MS) while the neutral polar fractions were also analysed using LC-MS APCI for GDGT characterization (Hopmans et al., 2004). These procedures were performed at the OGU (Organic Geochemistry Unit), University of Bristol. Individual organic compounds (or their derivatives) amenable to gas chromatography (GC) were identified in apolar, polar and acid fractions, and quantified relative to internal standards (5α-androstane, apolar fraction; hexadecan-2-ol, polar fraction; *n*-C_{19} alkane, acid fraction) using GC and gas chromatography–mass spectrometry (GC–MS). Typical error in absolute quantification was ±20%. GC analyses were performed on a CarloErba Gas Chromatograph equipped with a flame ionisation detector (FID) and fitted with a Chrompack fused silica capillary column (50 m × 0.32 mm i.d.) coated with a CP Sil-5CB stationary phase (dimethylpolysiloxane equivalent, 0.12 μm film thickness). GC–MS analysis was performed on a Thermoquest Finnigan Trace GC interfaced with a Thermoquest Finnigan Trace MS operating with an electron ionisation source at 70 eV and scanning over *m/z* ranges of 50 to 850 Da. The GC was fitted with a fused silica capillary column (50 m × 0.32 mm i.d.) coated with a ZB1 stationary phase (dimethylpolysiloxane equivalent, 0.12 μm film thickness). For both GC and GC–MS, 1 μl of sample was injected at 70 °C using an on-column injector. The temperature was increased to 130 °C with an initial ramp of 20 °C/min, then to 300 °C at 4 °C/min, followed by an isothermal hold for 20 min. To facilitate interpretation, various ratios of biomarkers indicative of organic matter source were calculated (see Table 1).

3.3. Stable carbon isotope analyses

Bulk organic carbon isotope analysis ($\delta^{13}C$) of 31 samples spanning from −60 cm to 1.31 m were performed at Stable Isotope Laboratory, GNS Science. Carbon isotopic compositions of methylated *n*-alkanoic acids were determined for all samples (26 samples) distributed along the 21.20 m-length the section. This was done via gas chromatography-combustion-isotope ratio mass spectrometry (GC-C-IRMS), at the OGU, University of Bristol, using a Hewlett Packard 6890 gas chromatograph connected to a Thermoquest Finnigan Delta plus XL spectrometer, via a GC III combustion interface (comprising Cu, Pt and Ni wires within a fused alumina reactor at a constant temperature of 940 °C). GC

Table 1
Ratios used in this study to examine changes in biomarkers distributions.

Ratio name	Mathematical Equation		Reference	Interpretation
High to Low Molecular Weight ratio of *n*-alkyl biomarkers (**HMW/LMW**)	HMW/LMW $_{n\text{-alkane}} = (\sum \geq C_{25})/(\sum \leq C_{21})$ HMW/LMW $_{n\text{-alkanoic acid}} = (\sum \geq C_{24})/(\sum \leq C_{20})$	HMW *n*-alkyl components display an odd-over-even (*n*-alkanes) or even-over-odd (*n*-alkanoic acids) indicative of a higher plant source	Eglinton and Hamilton (1967); Eglinton and Eglinton (2008)	Indicative of terrestrial (plant) vs aquatic sources
High Molecular Weight (**HMW**) *n*-alkly vs ∑total *n*-alkly ratio	$HMW_{n\text{-alkane}}/\sum$ total *n*-alkane $= (\sum C_{27-31})/(\sum$total *n*-alkane) HMW $_{n\text{-alkanoic acid}}/\sum$ total *n*-alkanoic acid $= (\sum C_{27-31})/(\sum$total *n*-alkanoic acid)		Cranwell et al. (1987); Eglinton and Hamilton (1967); Taylor et al. (2018)	Indicative of terrestrial (plant) sources
Low Molecular Weight (**LMW**) *n*-alkly vs ∑total *n*-alkly ratio	$LMW_{n\text{-alkane}}/\sum$ total *n*-alkane $= (\sum C_{13-21})/(\sum$total *n*-alkane) LMW $_{n\text{-alkanoic acid}}/\sum$ total *n*-alkanoic acid $= (\sum C_{12-30})/(\sum$total *n*-alkanoic acid)		Cranwell et al. (1987); Eglinton and Hamilton (1967); Taylor et al. (2018)	Indicative of marine (algae) sources
Terrigenous/aquatic ratio (**TAR**)	TAR $_{n\text{-alkane}} = (C_{27} + C_{29} + C_{31})/(C_{15} + C_{17} + C_{19})$ TAR $_{n\text{-alkanoic acid}} = (C_{24} + C_{26} + C_{28})/(C_{12} + C_{14} + C_{16})$		Bourbonniere and Meyers (1996); Cranwell et al. (1987)	Mathematically similar to HMW/LMW ratios and also related to terrestrial vs aquatic sources
Carbon preference index (**CPI**)	$CPI_{HMW\ n\text{-alkane}} = (2 \text{ x } \Sigma \text{ odd } C_{25-31})/(C_{24} + 2 \text{ x } (C_{26} + C_{28} + C_{30}) + C_{32})$ $CPI_{HMW\ n\text{-alkanoic acid}} = (2 \text{ x } \Sigma \text{ even } C_{26-32})/(C_{25} + 2 \text{ x } (C_{27} + C_{29} + C_{31}) + C_{33})$		Bray and Evans (1961); Peters et al. (2005)	Indicative of changes in terrigenous/aquatic contributions as well as degree of degradation and thermal maturity
Odd-over-even predominance (**OEP**) of *n*-alkanes	$OEP = C_{27} + (6 \text{ x } C_{29}) + C_{31}/(4 \text{ x } C_{28}) + (4 \text{ x } C_{30})$		Scalan and Smith (1970)	As Above
Even-over-odd predominance (**EOP**) of *n*-alkanoic acids	$EOP = C_{26} + (6 \text{ x } C_{28}) + C_{30}/(4 \text{ x } C_{27}) + (4 \text{ x } C_{29})$			
The higher plant *n*-alkane average chain length (**ACL**)	$ACL_{HMW\ n\text{-alkane}} = \Sigma(i*X_n)/\Sigma X_n$ $ACL_{HMW\ n\text{-alkanoic acid}} = \Sigma(i + 1*Xi+1)/\Sigma Xi + 1$	*Where i denotes the carbon-number of a given n-alkyl compound, ranging from 25 to 35, and X is its concentration*	Poynter and Eglinton (1990); Schefuß et al. (2003)	Shows changes in the distribution of HMW leaf waxes
Branched vs. isoprenoid tetraether (**BIT**) index	BIT = (bGDGT-I + bGDGT-II + bGDGT-III)/(bGDGT-I + bGDGT-II + bGDGT-III + crenarchaeol)	*Where I, II and III refer to brGDGTs with no rings and 4, 5 or 6 methyl groups, respectively*	Hopmans et al. (2004); Schouten et al. (2012)	Proxy for terrestrial organic matter (TOM) input into the marine environment
The **αβ/(αβ + ββ) ratio**	C_{31} [17α,21β/(17α,21β + 17β,21β)]	*Calculated from the* m/z *191 trace*	Mackenzie et al. (1980); Ourisson et al. (1979); Peters and Moldowan (1991); Seifert and Moldowan (1980)	Reflecting the thermal maturity of the section. It increases with thermal maturity
Sterane/hopane ratio **[S/(S + H)]**	Σ C_{27} + C_{28} + C_{29} steranes/(Σ C_{27} + C_{28} + C_{29} steranes + Σ C_{27} + … + C_{35} hopanes)	*Calculated from the* m/z *217 and 191 traces, respectively*	J Michael Moldowan et al. (1985b, 1985a)	Indicative of relative changes among eukaryotic and bacterial sources

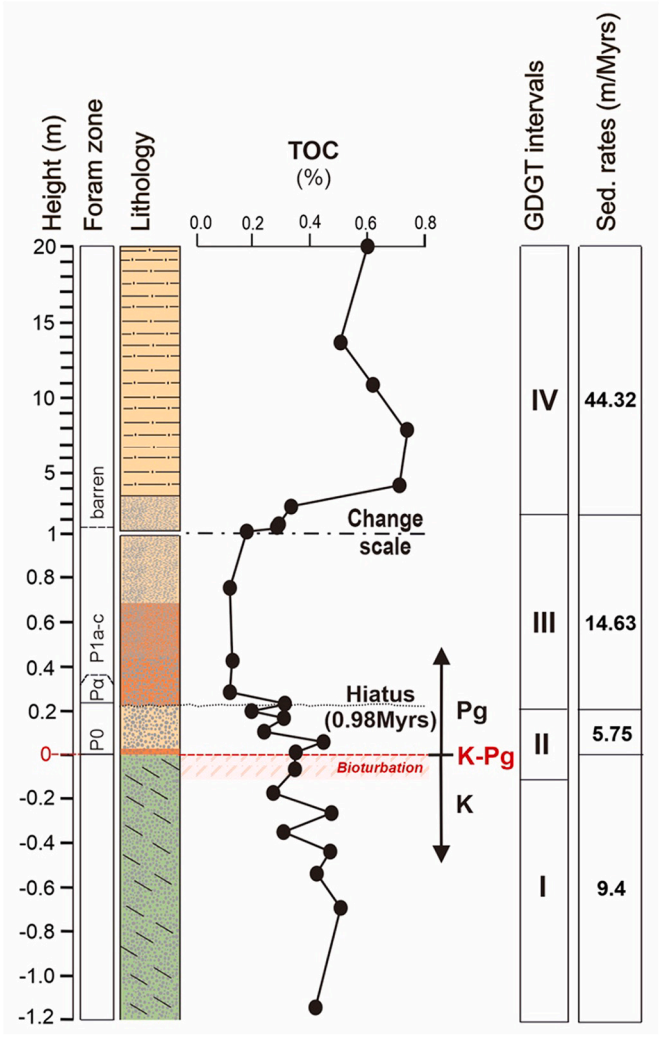

Fig. 2. TOC (%) at the mid-Waipara River K-Pg section (continuous black line). Modified from Taylor et al. (2018).

conditions were the same as described above for GC–MS. Duplicate or triplicate analyses were conducted for each sample, with values reported in standard delta (‰) notation relative to Vienna Pee Dee Bee Belemnite (VPDB). Analytical accuracy, on the basis of replicate analysis of a standard of mixed fatty acid methyl esters (FAMEs), was typically ±0.5‰ and precision, represented by 1 standard deviation is generally < ±0.5‰. For derivatized samples, standard mass balance correction procedures were used (Jones et al., 1991).

4. Results

Four stratigraphic intervals were previously defined for the mid-Waipara River section (I, II, III and IV; Fig. 2), based on the relative distributions of isoprenoidal glycerol dialkyl glycerol tetraether lipids (GDGTs) produced by pelagic Thaumarchaeota (Taylor et al., 2018). These intervals were inferred to represent distinct marine depositional environments in this section (Taylor et al., 2018), and the same zones are used here to interrogate ecological changes through the section. We refer to these intervals as zones herein. Zone I includes the uppermost Cretaceous from −1.2 to −0.15 m below K-Pg; Zone II spans −0.15 below to 0.215 m above K-Pg boundary; and Zones III and IV comprise the lower Paleocene from 0.215 to 2.75 m and from 2.75 to 20 m above K-Pg boundary, respectively. This top Cretaceous sample is within Zone II and treated as a Paleocene, due to down-working of Paleocene sediments by burrowing organisms (Fig. 2).

4.1. Total organic carbon (TOC)

TOC is <1% throughout the section (Table 2, Fig. 2). Values are variable and range from c. 0.27% to 0.51% in Zone I and from c. 0.19% to 0.45% in Zone II. They are lower above the unconformity at (0.215 m), c. 0.1% in Zone III, but increase to c. 0.2% to c. 0.7% in Zone IV. (Taylor et al., 2018).

4.2. Thermal maturity of mid-Waipara River section

As shown by Taylor et al. (2018), the organic matter in the mid-Waipara River section is thermally immature. Consistent with that, the 17β(H),21β-homohopane ($C_{31}\beta\beta$ hopane) and 17β(H),21β hopane ($C_{30}\beta\beta$ hopane) isomers are predominant (Mackenzie et al., 1980; Ourisson et al., 1979; Peters and Moldowan, 1991; Seifert and Moldowan, 1980), and the C_{31} αβ/(αβ + ββ) ratio (Table 2 and Fig. 3), is relatively low, ranging from 0.06 to 0.47. Intriguingly, the C_{31} αβ/(αβ + ββ) ratio varies throughout the section, despite no expected variation in thermal history. Higher ratios occur in Zones I, II and IV, while lower ratios occur in Zone III (Fig. 3B). Given the thickness of this section, it is unlikely that these values reflect thermal maturity variations of the rocks themselves.

The CPIs of the *n*-alkanoic acids are >2 and those of the *n*-alkanes are >1, also consistent with a low thermal maturity. They also vary through the section, exhibiting similar profiles (Tables 2 and 3 and Fig. 3B): lowest CPIs occur in Zones II and III, reaching a minimum in lower Zone III – at 0.425 m (f202) for *n*-alkanes and at 1.55 m (f218) for *n*-alkanoic acids. CPIs then increase into Zone IV reaching similar values to that of Zone I (Tables 2,3 and Fig. 3). These trends are opposite to those of the hopane isomers if governed by similar processes (i.e. delivery of petrogenic organic matter; Handley et al., 2010).

4.3. Biomarkers present in mid-Waipara River Sediments

Despite relatively low TOC contents (Fig. 2), the sediments in the mid-Waipara River K-Pg boundary section contain a full complement of hydrocarbons (i.e. *n*-alkanes, acyclic isoprenoidal, steranes, hopanes), polar compounds (i.e. GDGTs; Taylor et al., 2018), and fatty acids (i.e. *n*-alkanoic acids, hopanoic acids).

The apolar fractions typically contain a homologous series of *n*-alkanes (Table 2 and Fig. 4) with a relatively strong odd-over-even predominance. LMW *n*-alkanes ($\leq C_{21}$), typically attributed to aquatic sources (Cranwell et al., 1987; Gelpi et al., 1970), dominate throughout Zone III, whereas HMW homologues ($\geq C_{25}$) associated with terrestrial OM source dominate in Zone I, Zone II and Zone IV. Pristane and phytane occur in concentrations similar to those of co-occurring LMW *n*-alkanes (Fig. 4B) and exhibit similar variations through the section. The apolar fractions also contain a series of hopanes, ranging from C_{27} to C_{32} (Fig. 4C), as well as hop-13(18)-enes and hop-17(21)-enes, usually in concentrations similar to those of HMW *n*-alkanes (Fig. 4C). Steranes (C_{27}-C_{29}), tetracyclic triterpanes arising from diagenetic alteration of sterols (which were also observed in the polar fractions) and consequently deriving almost exclusively from eukaryotic organisms (e.g. Peters et al., 2005; Schwark and Empt, 2006 and references therein), were also observed. Also present in many samples is a pentacyclic triterpenoid, tentatively identified as taraxer-14-ene related with higher plants.

Acid fractions are dominated by a homologous series of *n*-alkanoic acids (Fig. 5) with a relatively strong even-over-odd predominance. In particular, the C_{16} and C_{18} homologues are predominant throughout much of the section, with subordinate maxima of the C_{22} and $C_{26–28}$ homologues (Fig. 5B). However, LMW ($\leq C_{20}$) compounds are less abundant than the HMW components in much of Zone I and through Zone IV. C_{30}, C_{31} and C_{32} 17,21-hopanoic acids occur at concentrations similar to or slightly greater than those of HMW ($\geq C_{24}$) *n*-alkanoic acids

Table 2
Total organic carbon content (TOC, %), *n*-alkanes, acyclic isoprenoids and taraxer-14-ene concentrations [μg/g dry weight (DW)] and main ratios across the mid-Waipara River section (New Zealand). The K-Pg boundary is indicated by the red dash line.

Distance K-Pg (m)	Sample	TOC (%)	GDGT Zones	Σ *n*-alkane	taraxer-14-ene	Pr + Ph	HMW	LMW	RATIOS Apolar fraccion						
									HMW/Σ *n*-alk	HMW/LMW	$\alpha\beta/(\alpha\beta+\beta\beta)$	ACL	TAR	CPI	OEP
20.000	f536	0.61		45	5.7	0	30	10	0.7	3.4	0.3	29	6.6	2.3	2.6
13.740	f537	0.50		70	0.9	5	40	20	0.5	1.6	0.3	29	2.7	2,0	2.5
10.840	f538	0.62	Zone IV	100	3.1	10	70	20	0.7	3.7	0.3	29	6.5	2.2	2.6
7.840	f539	0.74		20	0.7	10	10	5	0.6	2.6	0.2	29	4.4	2.1	2.7
4.110	f541	0.72		50	0.6	30	20	20	0.5	1.4	0.4	28	1.8	1.7	2.7
2.750	f232	0.34		390	0.2	520	10	370	0.0	0.0	0.3	28	0.0	1.6	2.3
1.550	f218	0.29		200	0.0	420	2	200	0.0	0.0	0.3	27	0.0	1.5	1.4
1.250	f215	0.27		1500	0.1	510	30	1500	0.0	0.0	0.3	28	0.0	1.5	1.5
1.050	f213	0.18	Zone III	100	0.1	480	4	90	0.0	0.1	0.3	28	0.0	1.6	1.9
0.750	f209	0.12		230	0.0	890	6	200	0.0	0.0	0.3	28	0.0	1.1	1.3
0.425	f202	0.13		300	0.0	370	10	300	0.0	0.0	0.3	26	0.0	0.8	0.3
0.275	f199	0.12		200	0.0	340	20	170	0.1	0.1	0.4	29	0.1	1.2	1.7
0.220	f554	0.32		100	0.1	190	10	80	0.1	0.1	0.4	29	0.1	1.4	1.7
0.190	f197	0.19		1100	0.1	1040	30	1100	0.0	0.0	0.4	28	0.0	1.8	2.1
0.160	f556	0.31		30	0.1	50	10	20	0.3	0.5	0.6	28	0.4	1.2	1.5
0.100	f558	0.23	Zone II	9	0.3	70	1	7	0.1	0.2	0.6	28	0.2	1.4	2.2
0.050	f559	0.45		30	0.3	70	2	300	0.1	0.1	0.6	28	0.1	1.4	2.2
0.005	f560	0.35		180	0.2	58	50	90	0.3	0.5	0.6	28	0.5	1.3	2.2
−0.070	f561	0.35		93	0.9	39	40	30	0.5	1.5	0.5	28	2,0	1.5	1.9
−0.180	f175	0.27		410	0.0	390	10	400	0.0	0.0	0.6	28	0.0	2.1	2.5
−0.273	f172	0.48		180	0.0	170	10	200	0.0	0.0	0.6	29	0.0	1.5	1.7
−0.355	f170	0.31	Zone I	670	0.2	690	40	600	0.1	0.1	0.6	27	0,0	1.3	2.5
−0.440	f168	0.47		390	0.1	490	20	360	0.1	0.1	0.6	28	0,0	1.9	2.8
−0.545	f165	0.43		270	0.0	430	4	270	0.0	0.0	0.6	29	0.0	2.3	2.9
−0.700	f161	0.51		410	0.1	600	20	390	0.1	0.1	0.6	29	0.1	1.8	2.2
−1.150	f562	0.42		150	0.6	200	40	80	0.3	0.5	0.6	28	0.4	1.6	2.7

through the mid-Waipara River section, with a predominance of 17β(H),21β-bishomohopanoic acid (C_{31}) (Fig. 5A), reflecting the relatively low thermal maturity of the studied section.

4.4. Depth profiles of terrestrial biomarkers

Total concentrations of *n*-alkanes range from 8.9 to 1500 ng g^{-1} dry weight (DW) of sediment (Table 2 and Fig. 6A). The *n*-alkane HMW/LMW ratio (as well as HMW/Total *n*-alkane and TARs) are variable but generally low in Zones I, II and III with the lowest ratios occurring in Zone III, coinciding with the lowest CPIs (Fig. 3B). Ratios are higher in Zone IV (Table 2 and Fig. 6B, C, D). Total concentrations of *n*-alkanoic acids range from 0.28 to 1300 ng g^{-1} dry weight (DW) of sediment (Table 3 and Fig. 6A). The *n*-alkanoic acid HMW/LMW ratio (and HMW/Total *n*-alkanoic and TARs ratios) are strongly variable in Zones I and II and then have low and constant values through Zone III. Ratios are slightly higher in Zone IV (Table 3 and Fig. 6B, C, D).

The BIT (Branched Isoprenoid Tetraether; Hopmans et al., 2004) index reflects terrestrial soil OM inputs and has been previously published for the mid-Waipara River section by (Taylor et al., 2018). It is relatively low (< 0.1; see Fig. 6E) throughout the section, indicating a relatively small terrestrial component of OM relative to marine (Hopmans et al., 2004; Weijers et al., 2006). Nonetheless, variations do occur, with values between 0.09 and 0.1 in Zones I and II, minimum values of 0.06 in zone III and slightly higher values (ca 0.08) in Zone IV (Fig. 6E).

Taraxer-14-ene and related pentacyclic triterpenoids are common in higher plants (e.g. Pancost and Boot, 2004), including for example, in some peat-forming plants (Pancost et al., 2002), mangrove leaves (Versteegh et al., 2004; Wannigama et al., 1981) and seagrass blades (Gillan et al., 1984). Concentrations of taraxer-14-ene are generally low throughout Zone I, from c. 0.03–0.89 μg/ g DW (Fig. 6F), with a slightly elevated value at −7 cm (f561), the last sample from the Cretaceous included in Zone II (which could reflect mixture from post K-Pg boundary sediments). Then, Taraxer-14-ene concentrations are generally higher in the post K-Pg boundary Zone II, it is entirely absent or low in concentration (<0.2 μg/ g) throughout Zone III, but occurs in higher and variable concentrations, from 0.61 to 5.69 μg/ g, in Zone IV (Fig. 6F).

4.5. Depth profiles of aquatic biomarkers

In the mid-Waipara River section, LMW *n*-alkane and *n*-alkanoic acid concentrations (and associated ratios) are rather variable (Tables 2 and 3), but trends are evident in LMW vs total *n*-alkane ratios (Fig. 7C). These are high in Zone I and then decrease into Zone II, then increase throughout Zone II achieving highest and stable values in zone III; and finally decrease into Zone IV. The pr + ph concentrations exhibit a similar profile, with high and variable values in Zone I, lowest values in Zone II, and an increase to the highest values in the section in zone III. They also decrease to lower values in Zone IV and are absent at 20 m above the K-Pg boundary (f536) (Table 2 and Fig. 7D). The LMW vs total alkanoic acid ratio exhibits some similar trends but overall, much higher variability (Fig. 7C). Sterane abundances, determined relative to hopanes as the sterane to hopane ratio [S/(S + H)], are also thought to reflect algal production (Moldowan et al., 1985b, 1985a). They exhibit dissimilar profiles in some respects, with the highest (albeit variable) ratios occurring in Zones I and III and low ratios occurring in Zones II and IV. However, they are similar to LMW *n*-alkane ratios and pr + ph concentrations, and all proxies suggest relatively low algal/aquatic inputs in Zone II (Fig. 7G).

The predominant three regular steranes, C_{27}-cholestane, C_{28}-ergostane and C_{29}-stigmastane, are present in all samples but only as the 5α,14α,17α,20R epimer, consistent with a low thermal maturity. Regular sterane (C_{27}, C_{28} and C_{29}) distributions (%) vary slightly through the section but with no clear trends (Fig. 7E). Typically, the C_{27} and C_{29} components have similar abundances and dominate over the C_{28} component. The 27/29 ratio (Fig. 7F) records similar abundances of C_{27} and C_{29} component for Zones I, II and III but then decreases to lower values into Zone IV.

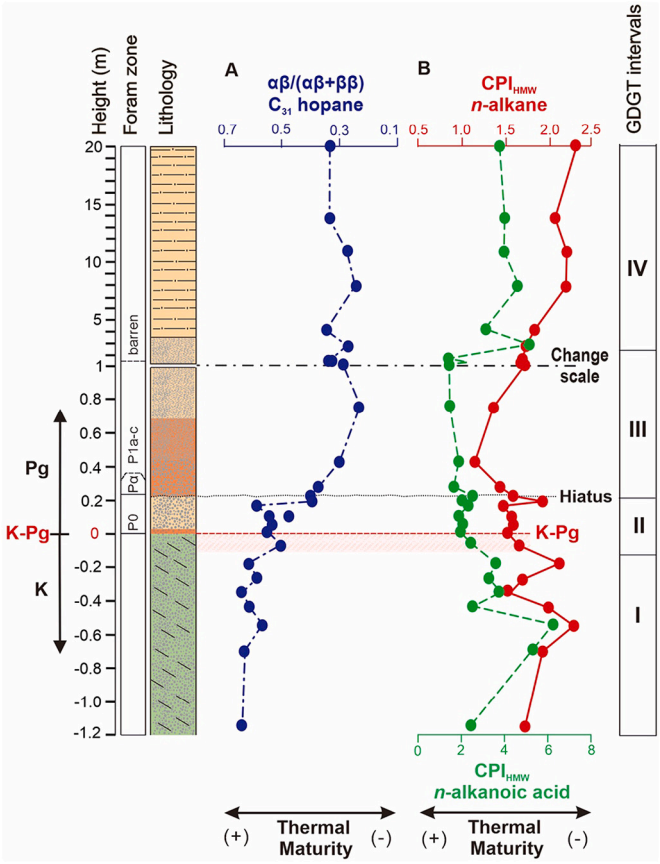

Fig. 3. – Biomarker ratios indicative of thermal maturity or organic matter alteration at the mid-Waipara River K-Pg section. (A) αβ/(αβ + ββ) C_{31} hopane ratio (dashed blue line). Black arrows show higher (+) or lower (−) alteration/thermal maturity (note reversed axis) (B) Carbon preference index (CPI_{HMW}) of *n*-alkanes (continuous red line) = (2 x Σ odd (C_{25-31})/(C_{24} + 2 x (C_{26}+ C_{28} + C_{30}) + C_{32}) and Carbon preference index (CPI_{HMW}) of *n*-alkanoic acids (dashed green line) = (2 x Σ even (C_{26-32})/(C_{25} + 2 x (C_{27} + C_{29} + C_{31}) + C_{33}) (Bray and Evans, 1961). (For interpretation of the references to colour in this figure legend, the reader is referred to the web version of this article.)

4.6. Bulk organic matter carbon isotopic compositions

Bulk organic matter ($\delta^{13}C_{TOC}$) values from 31 samples spanning from −1.15 cm to 1.31 m, are relatively stable (Fig. 8A and table in supplementary material), ranging from c. -28 ‰ to −29 ‰ through the Zone I. There is no apparent change associated with the K-Pg boundary horizon at 0 cm. A transient positive shift to c. -24 ‰ occurs 5 cm above the boundary. $\delta^{13}C_{TOC}$ values then decrease in the overlying 3 samples to c. – 26.5 ‰ and then return to values similar to the Maastrichtian values (at c. -28 ‰ to −29‰) from 10 cm above the K-Pg boundary (Zone II) and remain relatively invariant at Zones III and IV.

4.7. Biomarker carbon isotopic compositions

Carbon isotopic compositions of individual lipids reflect both the isotopic composition of the carbon source utilized by the organism and the isotopic fractionations accompanying carbon fixation and biosynthesis, which are, in turn, dependent on environmental conditions and biology (e.g. Hayes, 1993). Here, we focus on high molecular weight (HMW; C_{26}-C_{34}) and low molecular weight (LMW; C_{14}-C_{18}) *n*-alkanoic acids, likely reflecting higher plant and mixed algal sources, respectively. We used *n*-alkanoic acids instead *n*-alkanes because the former are more abundant in this section.

4.7.1. High molecular weight n-alkanoic acids

The carbon isotopic compositions ($\delta^{13}C$) of HMW even-carbon-number *n*-alkanoic acids (Fig. 8B) likely reflect higher plant signals (Fig. 8B and Table 3). The mean-weighted $\delta^{13}C_{HMW}$ values increase through Zone I, from c. -32‰ to −29‰, varying by c. 3 ‰. In Zone II, the mean $\delta^{13}C$ values of *n*-alkanoic acids are generally lower than those of Zone I, varying from −33‰ to −28 ‰, and similar values persist into Zone III (−30 ‰ to −33 ‰). The $\delta^{13}C_{HMW}$ values are higher and stable, like those of the Maastrichtian (c. -31 ‰ to −30 ‰), in Zone IV. This trend is also reflected in the $\delta^{13}C$ values of individual HMW *n*-alkanoic acids.

4.7.2. Low molecular weight n-alkanoic acids

Although sources of LMW (C_{14}-C_{18}) *n*-alkanoic acids are more ambiguous than the HMW counterparts, their abundance depth profiles parallel those of pristane and phytane suggesting an aquatic, potentially algal, source. We show the mean weighted average $\delta^{13}C$ records of individual C_{14}, C_{16} and C_{18} *n*-alkanoic acids ($\delta^{13}C_{LMW}$) (Fig. 8C and Table 3). The Maastrichtian sediments of Zone I are characterized by relatively high and variable *n*-alkanoic acid $\delta^{13}C_{LMW}$ values that range from c − 29 ‰ to −25 ‰. Then in Zone II, $\delta^{13}C_{LMW}$ values decrease to a mean value of c. -29 ‰ and remain relatively stable, including into Zone III where they vary from −29 ‰ to −32 ‰. They return to higher and stable values of c. -28 ‰ to −31 ‰ in Zone IV.

5. Discussion

There have been several biomarker studies on the biotic response and recovery after the K-Pg boundary in distal sections (Bralower et al., 2020; Sepúlveda et al., 2009; Taylor et al., 2018; Sosa-Montes de Oca et al., 2021), as well as recent papers on the biotic response within the Chicxulub structure (Schaefer et al., 2020). The findings of these studies differ, however, the response of non-fossilizing plankton appears to be spatially variable. Here, we interpret biomarker abundance and distribution across the K-Pg boundary at the mid-Waipara River section (MW), as well as the carbon isotopic composition of TOC and specific biomarkers (HMW and LMW *n*-alkanoic acid), to explore changes in OM source. We then focus on algal biomarkers to specifically examine the marine biotic response and compare those trends, where possible, to those observed at other sites.

5.1. Changes in organic matter assemblages across the K-Pg boundary

Biomarker distributions in the mid-Waipara River section indicate complex changes in the sources of organic matter, including across the K-Pg boundary and during subsequent times. Overall, biomarkers indicate a mixed source assemblage between terrestrial, marine, and reworked petrogenic OM, as is expected in a marine section with abundant terrestrial palynomorphs, but their relative proportions change through all section, and in particular across the K-Pg boundary. A terrestrially derived source of OM is corroborated by long-chain *n*-alkyl compounds, HMW *n*-alkanes with a relatively high odd-over-even predominance and HMW *n*-alkanoic acids with a high even-over-odd predominance, indicating a significant terrigenous input of organic matter to the sediments (Cranwell et al., 1987; Eglinton and Clavin, 1967; Eglinton and Hamilton, 1967; Kvenvolden, 1967; Rieley et al., 1991). This is also supported by the high abundance of terrestrial palynomorphs (Vajda et al., 2001; Vajda and Raine, 2003a), the presence of taraxer-14-ene (Versteegh et al., 2004), and the presence, albeit in low abundances, of branched GDGTs which indicate fluvially transported soil OM input (Fig. 6 and Table 2).

Nonetheless, evidence for marine OM inputs is suggested by LMW *n*-alkyl compounds (e.g., Ali and Mudge, 2006; Carrie et al., 1998) that are often more abundant than their HMW counterparts, abundant pristane and phytane in some intervals (e.g., Dean and Whitehead, 1961; Rontani and Volkman, 2003), and high proportions of C_{27} steranes (e.g., Huang

Table 3
Total organic carbon content (TOC, %), main *n*-alkanoic acid concentration [μg/g dry weight (DW)], ratios and carbon isotopic data (‰) across the mid-Waipara River section (New Zealand). The K-Pg boundary is indicated herein in red dash line.

Distance K-Pg (m)	Sample	TOC (%)	GDGT Zones	Σ n-alkanoic acid	HMW	LMW	RATIOS *n*-alkanoic acid						Carbon Isotopic data	
							HMW/Σ *n*-alk	HMW/LMW	ACL	TAR	CPI	OEP	$\delta^{13}C_{HMW}$	$\delta^{13}C_{LMW}$
20.000	f536	0.61		410	80	280	0.2	0.3	29	0.3	3.8	3.6	−29.2	−30.9
13.740	f537	0.50		590	110	4100	0.2	0.3	29	0.3	4.0	3.9	−30.0	−31.1
10.840	f538	0.62		710	140	490	0.2	0.3	29	0.3	4.0	3.7	−29.8	−30.9
7.840	f539	0.74		360	30	320	0.1	0.1	28	0.5	4.7	4.3	−29.6	−30.1
4.110	f541	0.72	Zone IV	70	20	30	0.3	0.8	28	1.4	3.1	3.1	−27.8	−30.5
2.750	f232	0.34		750	190	460	0.3	0.4	28	0.5	5.2	4.1	–	−33.2
1.550	f218	0.29		230	10	200	0.1	0.1	27	0.1	1.4	1.4	−31.4	−30.1
1.250	f215	0.27		1030	12	990	0.0	0.0	28	0.0	2.3	2.4	−31.5	−30.0
1.050	f213	0.18		290	4	270	0.0	0.0	27	0.0	1.5	1.6	−34.6	−30.5
0.750	f209	0.12		370	25	300	0.1	0.1	27	0.1	1.5	1.6	−31.5	−31.8
0.425	f202	0.13		1300	44	1200	0.0	0.0	27	0.1	1.9	2.0	−29.3	−33.2
0.275	f199	0.12		930	40	800	0.0	0.1	27	0.1	1.7	1.8	−29.8	−33.0
0.220	f554	0.32	Zone III	870	20	830	0.0	0.0	28	0.0	2.5	2.6	−29.1	−30.4
0.190	f197	0.19		1100	60	940	0.1	0.1	27	0.1	2.1	2.0	−32.0	−32.7
0.160	f556	0.31		18	5	6	0.3	0.9	27	3.0	2.4	2.4	−28.8	−29.8
0.100	f558	0.23		370	30	290	0.1	0.1	28	0.2	1.9	2.0	−29.2	−31.7
0.050	f559	0.45		130	12	100	0.1	0.1	27	0.2	2.1	2.2	−29.1	−30.7
0.005	f560	0.35	Zone II	300	80	91	0.3	0.9	27	5.8	2.0	2.2	−26.0	−32.0
−0.070	f561	0.35		90	7	70	0.1	0.1	28	0.2	2.5	2.6	−29.3	−28.7
−0.180	f175	0.27		200	25	150	0.1	0.2	29	0.3	3.6	4.0	−26.5	−29.7
−0.273	f172	0.48		120	70	20	0.6	3.1	28	9.7	3.3	3.4	−25.2	−28.7
−0.355	f170	0.31		30	2	30	0.1	0.1	28	0.1	3.9	4.1	−27.9	−30.5
−0.440	f168	0.47		1	0	0	0.4	1.2	28	3.8	2.6	2.3	−28.0	−30.0
−0.545	f165	0.43		93	75	10	0.8	6.4	29	15.6	6.3	3.9	−26.4	−30.9
−0.700	f161	0.51		0	0	0	0.5	1.1	28	2.6	–	–	−29.0	–
−1.150	f562	0.42	Zone I	50	21	10	0.4	1.6	27	4.4	2.5	2.4	−29.2	−32.4

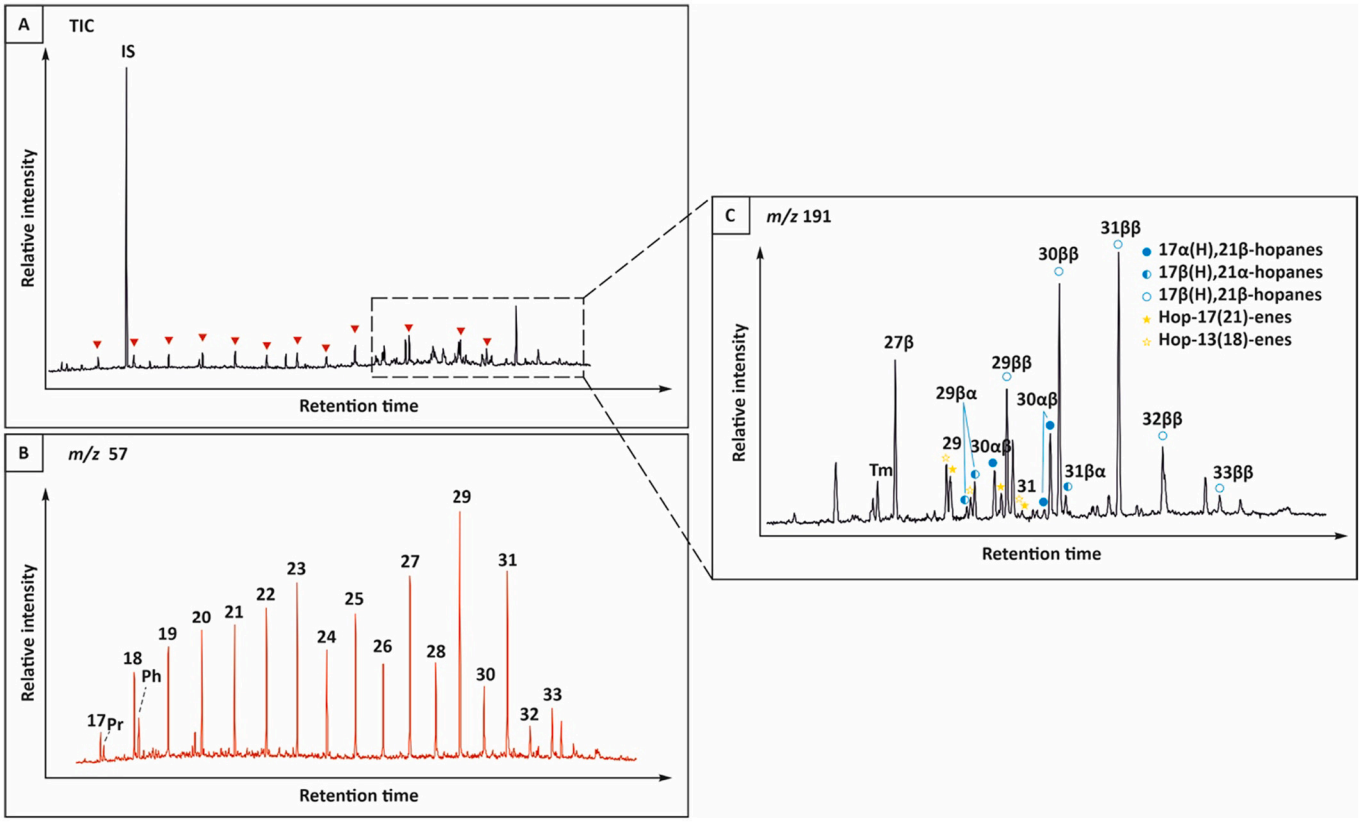

Fig. 4. Apolar fraction of Paleocene sample M34/f539 (7.84 m, Zone IV). (A) Total ion current (TIC) chromatogram. (B). *m/z* 57 mass chromatogram showing predominantly *n*-alkanes. Numbers correspond to carbon chain length, I·S = internal standard (5α-androstane) and Pr = pristane, Ph = phytane. (C) Hopanes and hopenes shown by the *m/z* 191 mass chromatogram. Numbers correspond to number of carbon atoms in hopane/hopene structure, annotated with the stereoisomeric configuration at the C-17 and C-21 positions.

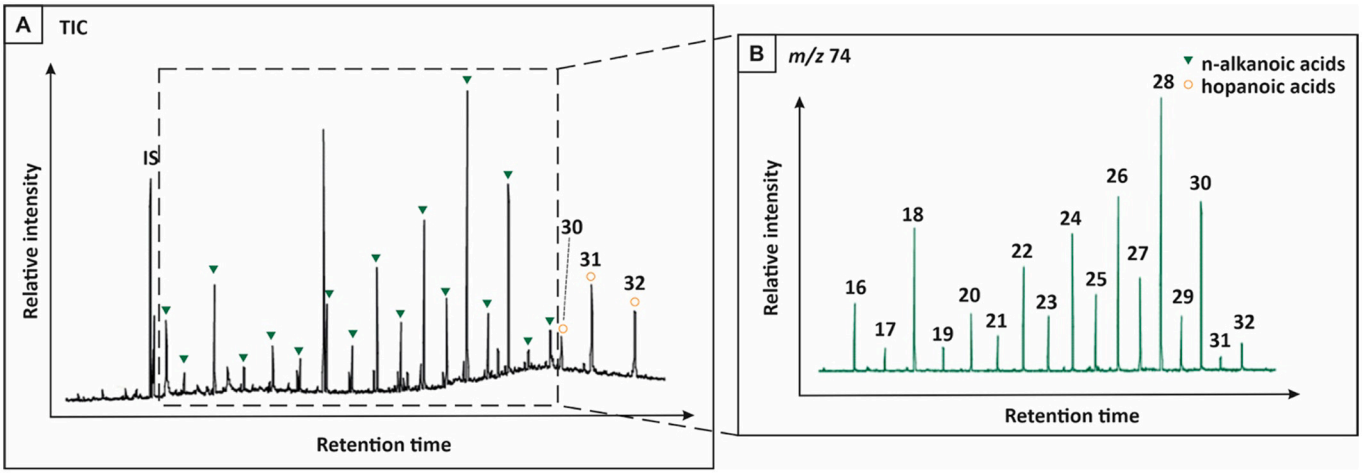

Fig. 5. Methylated acid fraction of uppermost Cretaceous sample f172 (−27 cm, Zone I). (A) Partial total ion current (TIC) chromatogram. I·S = internal standard (5α-androstane). Numbers above the hopanoids correspond to the number of carbon atoms in the non-methylated hopanoic acid; all labelled hopanoic acids occur in the 17b(H),21b configuration. (B) The partial *m/z* 74 mass chromatogram showing *n*-alkanoic acids, with numbers above peaks corresponding to the carbon chain length.

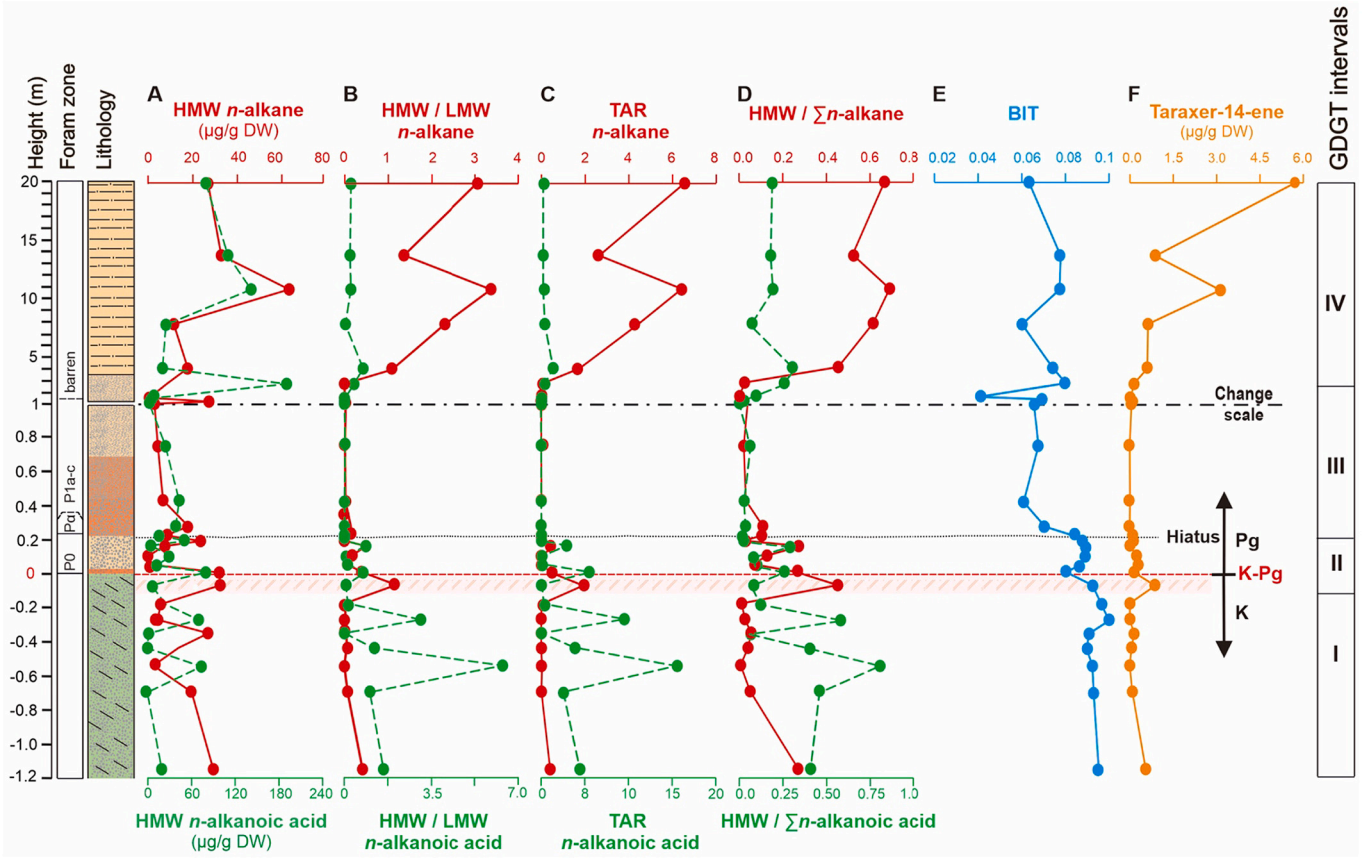

Fig. 6. Concentrations and ratios of terrestrial biomarkers through the mid-Waipara River K-Pg section. (A) High molecular weight (HMW) *n*-alkanes ($\geq C_{25}$) (continuous red line) and *n*-alkanoic acids ($\geq C_{24}$) (dashed green line) concentrations (µg/g DW). (B) HMW/LMW ratios of *n*-alkanes (continuous red line) and *n*-alkanoic acids (dashed green line). (C) terrigenous/aquatic ratios (TAR; Cranwell et al., 1987; Bourbonniere and Meyers, 1996) of *n*-alkanes $[C_{27} + C_{39} + C_{31}]/[C_{15} + C_{17} + C_{19}]$ (continuous red line) and *n*-alkanoic acids $([C_{24} + C_{26} + C_{28}]/[C_{14} + C_{16} + C_{18}])$ (dashed green line). (D) HMW *n*-alkane/∑total *n*-alkane ratio $([C_{24} + C_{26} + C_{27} + C_{28} + C_{29} + C_{30} + C_{31} + C_{32} + C_{33} + C_{34} + C_{35} + C_{36} + C_{37}]/[\sum$ total *n*-alkane]) (continuous red line) and HMW *n*-alkanoic acid/∑total *n*-alkanoic ratio $([C_{25} + C_{26} + C_{27} + C_{28} + C_{29} + C_{30} + C_{31} + C_{32} + C_{33} + C_{34} + C_{35} + C_{36}]/[\sum$ total *n*-alkanic acid]) (dashed green line). (E) BIT index (BIT = [bGDGT-I + bGDGT-II + bGDGT-III)/(bGDGT-I + bGDGT-II + bGDGT-III + crenarchaeol]) (continuous blue line). (F) taraxer-14-ene concentrations (µg/g DW) (continuous orange line). Depth is presented relative to GDGT Zones established in Taylor et al., 2018. The K-Pg boundary is indicated herein in red dash line. (For interpretation of the references to colour in this figure legend, the reader is referred to the web version of this article.)

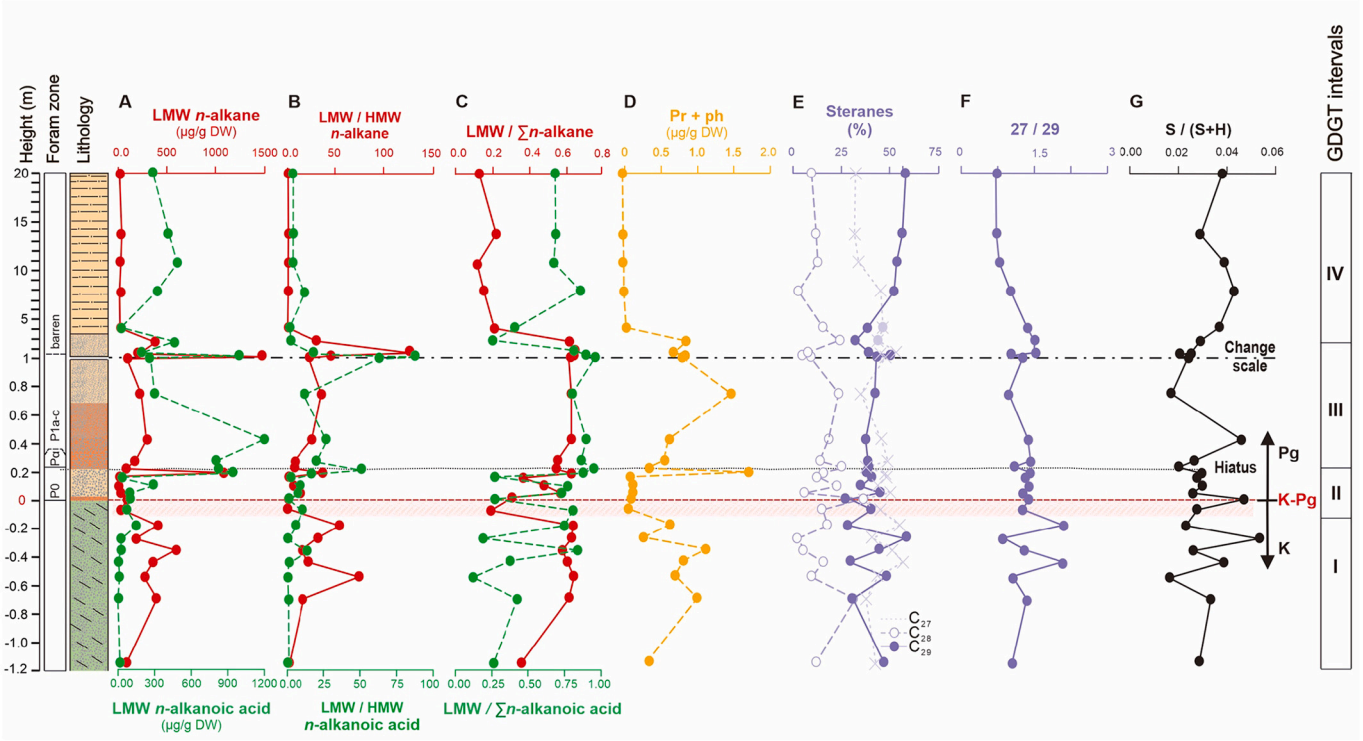

Fig. 7. Concentrations and ratios of marine biomarkers throughout the mid-Waipara River K-Pg section. (A) Low Molecular Weight (LMW) *n*-alkanes ($\geq C_{25}$) and *n*-alkanoic acids ($\geq C_{24}$) concentrations (µg/g DW). (B) LMW/HMW ratios of *n*-alkanes (continuous red line) and *n*-alkanoic acids (dashed green line). (C) LMW *n*-alkane/$\sum$total *n*-alkane ratio ($[C_{13} + C_{14} + C_{15} + C_{16} + C_{17} + C_{18} + C_{19} + C_{20} + C_{21}]/[\sum$ total *n*-alkane]) (continuous red line) and LMW *n*-alkanic acid/$\sum$total *n*-alkane ratio ($[C_{12} + C_{13} + C_{14} + C_{15} + C_{16} + C_{17} + C_{18} + C_{19} + C_{20}]/[\sum$ total *n*-alkanic acid]) (dashed green line). (D) Sum of pristane (Pr) and phytane (Ph) concentrations (µg/g DW) (dashed orange line). (E) % of each regular sterane [$C_{27}/\Sigma(C_{27} + C_{28} + C_{29})$; $C_{28}/\Sigma(C_{27} + C_{28} + C_{29})$; $C_{29}/\Sigma(C_{27} + C_{28} + C_{29})$] (purple colours). (F) 27/29 ratio (continuous purple line). (G) sterane/hopane ratio (S/S + H) [$\Sigma (C_{27} + C_{28} + C_{29})/(C_{27} + C_{28} + C_{29}) + (\Sigma C_{27} + \ldots + C_{32})$] (continuous blue line). (For interpretation of the references to colour in this figure legend, the reader is referred to the web version of this article.)

and Meinschew, 1979) (Fig. 7; table in supplementary material). In addition, the presence of crenarchaeol and low BIT indices (Taylor et al., 2018) suggest a robust marine archaeal OM input. The BIT index is a proxy for the input of terrestrial OM – and especially soil OM – into aquatic environments (Hopmans et al., 2004), and typical values in terrestrial soils and marginal marine sediments are >0.9, whereas in open marine settings they are usually below 0.6 (Weijers et al., 2006). Values are always below 0.1 in this part of the mid-Waipara River section (only exceeding 0.1 in the late Paleocene and Eocene, Pancost et al., 2013), suggesting a strong aquatic (marine) input and minor soil organic matter input. Because the Thaumarchaeota that produce crenarchaeol are thought to sink relatively slowly, low BIT indices are also thought to indicate an active biological pump (Taylor et al., 2018). Crucially, the persistence of low-molecular weight (LMW) *n*-alkanes (C_{13}–C_{21}) and *n*-alkanoic acids (C_{12}–C_{20}) (Fig. 7; Tables 2 and 3), the putative algal chlorophyll degradation products pristane and phytane, and crenarchaeol is consistent with a persistent production and delivery of algal OM even in the aftermath of the K-Pg impact.

A third pool of OM inputs is likely reworked petrogenic organic matter as indicated by changes in the thermal maturity parameters in an otherwise thermally immature and stratigraphically short section. Crucially, an increase input of thermally mature organic matter, e.g. Zone I, II and IV, demands caution in interpreting some biomarker parameters, especially those based on *n*-alkanes which could be biased towards LMW homologues when petrogenic inputs are significant (Diefendorf et al., 2015). Indeed, terrestrial vs aquatic parameters based on *n*-alkanes often differ from those based on *n*-alkanoic acids (Figs. 6 and 7), and we are especially cautious where anomalously low HMW/LMW *n*-alkane ratios coincide with higher C_{31} hopane αβ/(αβ + ββ) ratios (Zones I and II). In addition, this reworked petrogenic organic matter could impact $\delta^{13}C_{TOC}$ values and this is explored below.

Although all three of these inputs of OM (terrestrial, marine and reworked petrogenic) are persistent, their relative proportions vary throughout the section. In Zone I, the *n*-alkanoic acid ratios indicative of terrestrial OM (HMW/LMW, TAR, HMW/$\sum$ *n*-alkanoic acid) are high but variable (Fig. 6B–D). This indicates that terrestrial OM input is generally high and periodically dominant, which is consistent with the generally lower concentrations of LMW *n*-alkanoic acids (Fig. 7A–C) and the relatively high CPIs for both *n*-alkanoic acids and *n*-alkanes. Relatively high terrestrial input is also consistent with the relatively high BIT indices in Zone I, although these values are still low overall and indicate that terrigenous inputs are primarily plant rather than soil derived. Although the equivalent *n*-alkane ratios (HMW/LMW, TAR, HMW/$\sum$ *n*-alkane acid) are low (Fig. 6B, C, D), superficially suggesting low plant inputs or changes in plant populations (Diefendorf et al., 2011), we attribute that to the influence of petrogenic inputs (Handley et al., 2010).

In Zone II, just after the K-Pg boundary, the *n*-alkanoic terrestrial to aquatic ratio decreases slightly as does the BIT index. TOC and pr + ph concentrations also decrease; whereas LMW *n*-alkane and *n*-alkanoic acid concentrations are variable but do not show a significant increase (Fig. 7 and Tables 2 and 3). The sterane/hopane ratio [S/(S + H)] (Fig. 7 and Table 2) variation is small (a decrease from 0.05 to 0.03 on a scale of 0 to 1). The lack of clear evidence for a significant decrease in aquatic (marine algal) inputs is consistent with the increase in the *proto-peridinioid* dinoflagellate species, *T. evittii* within Zone II (Taylor et al., 2018). Similar increases have been recorded at several other sites worldwide within planktonic foraminiferal Zone P0 and interpreted as an increase in primary productivity (e.g., Vellekoop et al., 2017). However, the species is also associated with warm surface waters and its

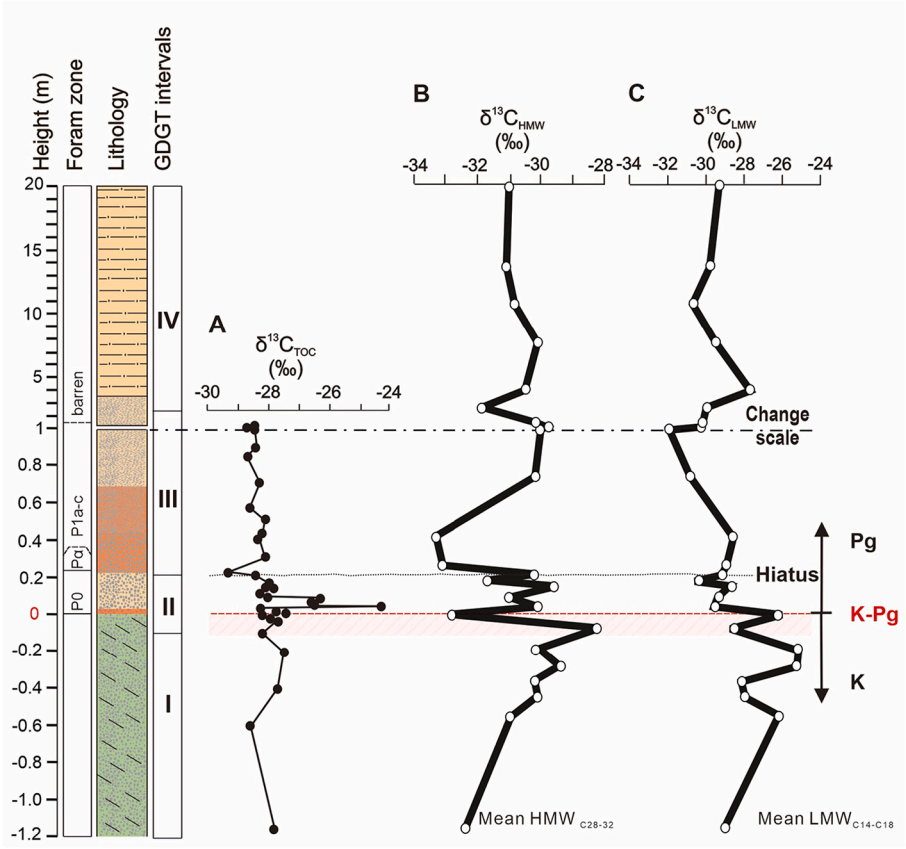

Fig. 8. Carbon Isotopic data at the mid-Waipara River K-Pg section (A) Carbon isotopic compositions of bulk organic carbon ($\delta^{13}C_{TOC}$). (B) Carbon isotopic compositions of high molecular weight alkanoic acids ($\delta^{13}C_{HMW}$). (C) Carbon isotopic compositions of low molecular weight alkanoic acids ($\delta^{13}C_{LMW}$).

increase in middle and higher latitudes is also attributed to warmer conditions (Taylor et al., 2018). In summary, this interval records an increase in petrogenic OM, a decrease in terrestrial OM and a variable signal for marine OM in which overall aquatic indicators show a decrease but some algal elements (dinoflagellates) indicate an increase in productivity.

This interval is also coincident with the 'fern spike' in New Zealand, identified from palynological analysis (Vajda et al., 2001; Vajda and Raine, 2003b). The fern spike is thought to reflect an early successional vegetation dominated by ferns, such as those following mass-kill of climax communities by volcanoes (Tschudy et al., 1984; Wolfe and Upchurch, 1987). Although mass-kill from volcanic eruptions typically results in a localized vegetation impact, more global impacts associated with the K-Pg bolide could include global darkness, cooling and subsequent warming, wildfires, SO_x and/or NO_x poisoning, dust and acid rain (Alvarez et al., 1980; Arinobu et al., 1999; Lyons et al., 2020; Smit, 1999; Toon et al., 1997), all of which could have impacted distal locations such as New Zealand. Such a mass-kill event could be represented by the dramatic decrease in some higher plant biomarker concentrations in Zone II. Although BIT values decrease from Zone I to Zone II, the shift is small, suggesting that decreased higher plant inputs reflect a smaller terrestrial biomass rather than a change in erosion and transport processes. The recolonization of the terrestrial biosphere in New Zealand is considered to have been relatively rapid, based on the pollen record (Vajda et al., 2001; Vajda and Raine, 2003a). However, the pollen record of the K-Pg boundary at other sites, e.g. the Raton Basin (North America), indicates a lower level of extinction than the leaf megafossil record, possibly due to extinction of groups which do not have pollen or have generalised pollen that is not diagnostic to specific or generic levels (Wolfe and Upchurch, 1987). Thus, terrestrial biomass reduction at mid-Waipara River could be greater than estimated from the pollen record, providing an explanation for suppressed concentrations of higher plant biomarkers through Zone II. Alternatively, the impact of the mass-kill on biomarker concentrations in Zone II could have been more indirect, e.g. via a change in the higher plant community (Diefendorf et al., 2011).

Across the unconformity between Zones II and III, BIT indices and *n*-alkanoic acid terrestrial to aquatic ratios decrease further; *n*-alkane terrestrial to aquatic ratios also decrease to their lowest values in the section. These shifts likely reflect lower inputs of soil and terrestrial plant OM to the sediment. Given that the unconformity spans an interval of ~1 myr, there are several possible explanations for this decrease in terrestrial inputs. The unconformity is linked to climatic cooling and an associated fall in relative sea level, which would be expected to increase terrestrial erosion and terrigenous input (Taylor et al., 2018). However, the overlying sediments record the subsequent climatic amelioration and transgression and this might explain the reduced terrestrial input. Cooler climatic conditions may have also been associated with lower precipitation and run-off. Drier conditions are also inferred from the conifer-dominated palynoflora within Zone III (Vajda and Raine, 2003b).

The C_{31} hopane $\alpha\beta/(\alpha\beta + \beta\beta)$ ratio decreases dramatically in Zone III (Fig. 3A), so we suggest it reflects a decrease, relative to Zones I and II, in the proportional input of reworked, petrogenic carbon (e.g. Carmichael et al., 2018; Castro et al., 2019; Hackley et al., 2020; Lyons et al., 2020; van Breugel et al., 2007). This is consistent with both the high terrigenous inputs inferred for Zones I and II, which could have been associated with erosion and weathering of reworked kerogen, as well as the elevated aquatic inputs inferred for Zone III which could have diluted allochthonous petrogenic carbon inputs. Given that interpretation, it is interesting to note that there is no major change in the C_{31} hopane $\alpha\beta/(\alpha\beta + \beta\beta)$ ratio across the K-Pg boundary itself.

Zone III also experienced dramatic changes in algal biomarkers.

Although TOC contents decrease, the concentrations of pr + ph, LMW *n*-alkanoic acids and *n*-alkanes, and S/(S + H) ratios increase, suggesting that primary productivity has recovered. However, this Zone is also where some of us (Taylor et al., 2018) had interpreted unusual changes in GDGT distributions as a disruption to the biological pump and this is discussed in 5.2 in the context of the post-K-Pg boundary aquatic recovery.

In Zone IV, most biomarker ratios return towards pre-K-Pg boundary conditions. The *n*-alkanoic acid and *n*-alkane terrestrial to aquatic ratios increase. C_{31} hopane αβ/(αβ + ββ) ratios also increase. BIT indices are slightly higher than in Zone III, although they remain lower than in Zones I and II. Concentrations of pr + ph are low and S/(S + H) ratios increase slightly, similar to what is observed in Zone II. Moreover, some differences in especially higher plant biomarkers have emerged: HMW to LMW *n*-alkane ratios are higher than in Zone I, whereas HMW to LMW *n*-alkanoic ratios are lower; taraxer-14-ene abundances are much higher than throughout the entire section. These suggest a recovery but also reorganisation of the terrestrial vegetation (Diefendorf et al., 2011). Intriguingly, the pollen record suggests a decrease in terrestrial inputs from 8 m above the boundary, based on the dominance of dinoflagellate cysts over terrestrial palynomorphs (Vajda and Raine, 2003b). Biomarkers and pollen have different taphonomies and can be transported from land to the marine environments in different ways (i.e., via aeolian or fluvial transport). Preservation and sedimentation rates, winnowing and changes in plant communities also differentially affect pollen and plant biomarker burial (e.g. Schouten et al., 2007). In any case, the concentrations of both LMW and HMW *n*-alkanoic acids (and other biomarkers) are relatively high, suggesting that both marine and terrestrial contributions to the sediment are persistent or increasing through Zone IV, consistent with the maximum in TOC content (Fig. 2).

5.2. Recovery of algal communities after K-Pg boundary

Bioturbation in the mid-Waipara River section means that the uppermost sample from the Cretaceous likely contains a Paleocene biomarker signature (Zone II). Accounting for that effect, the K-Pg boundary is characterized by a dramatic decrease in pr + ph concentrations and LMW/HMW *n*-alkane ratios, and a slight decrease in S/(S + H) ratios (Fig. 7). All of these suggest a significant decrease in aquatic inputs and possibly in marine productivity (Cranwell et al., 1987; Eglinton and Clavin, 1967; Eglinton and Hamilton, 1967; Kvenvolden, 1967; Rieley et al., 1991). However, concentrations of LMW *n*-alkanoic acids do not decrease, nor do the associated *n*-alkanoic acid ratios. Moreover, sterane distributions are remarkably stable, unlike variations observed in other distal settings (Sosa-Montes de Oca et al., 2021), and as mentioned above, increased proportions of *T. evittii* is evidence for increased productivity. These observations collectively mitigate against a simplistic interpretation of a post K-Pg boundary productivity collapse.

All of these biomarker signatures recover in Zone III and some of them recover in the uppermost sample from Zone II, suggesting that any

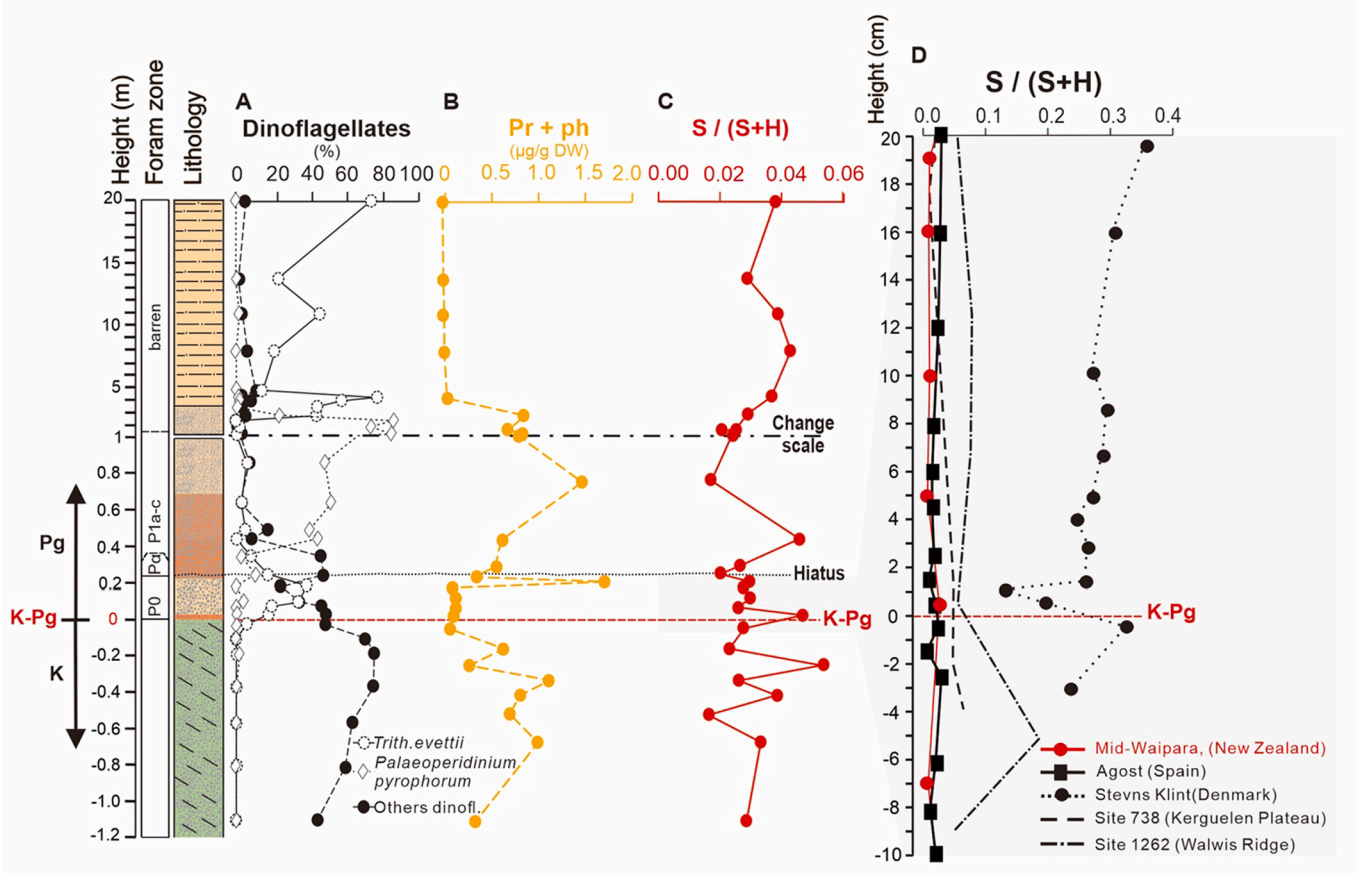

Fig. 9. Comparison of algal recovery at the mid-Waipara River K-Pg section. (A) % of dinoflagelates species in mid-Waipara River section from Taylor et al., 2018, *Trith. evettii* (continuous black line), *Palaeoperidinium pyrophorum* (dashed black line), and other dinoflagellates (dotted black line). (B) Sum of pristane (Pr) and phytane (Ph) concentrations (μg/g DW) (dashed orange line). (C) Sterane/hopane ratio (S/S + H) [Σ (C_{27} + C_{28} + C_{29})/(C_{27} + C_{28} + C29) + (ΣC_{27} + … + C_{32})] in mid-Waipara River section (continuous red line). (D) comparison of S/(S + H) ratio in different sections, in red colour for the mid-Waipara River section (this work) and in black colours for the Agost section (data from Sosa-Montes de Oca et al., 2021) (continuous black line), Stevn Klint section (data from Sepulveda et al. [2009]) (dotted black line), and sites 738 and 1262 (data from Bralower et al., 2020) (dashed and dashed-dotted black lines, respectively). Note that S/(S + H) ratios have been calculated using different MS fragmentation ions, such that differences in absolute values are meaningless. (For interpretation of the references to colour in this figure legend, the reader is referred to the web version of this article.)

decrease in primary productivity was transient. This is particularly noteworthy if previous indications of an increase in export productivity from the subsurface rather than surface waters during deposition of Zone III are correct (Taylor et al., 2018); primary productivity must have recovered to have overcome the effects of a less efficient biological pump. High marine productivity in Zone III relative to Zones I and II is also indicated by elevated Si/Al and Ba/Al ratios (Hollis and Strong, 2003), suggesting enhanced siliceous productivity. Furthermore, the TEX_{86}-derived SSTs (Sea Surface temperatures) (Taylor et al., 2018)); and the dinoflagellate acme of *Palaeoperidinium pyrophorum* coinciding with Zone III (Fig. 9A) both indicate cooler water and probable upwelling conditions (Willumsen, 2000, 2006), which could enhance surface primary productivity (Lyle, 1988; Meyers, 1997). The trends in biogenic silica correlate to similar intervals at other K-Pg boundary sections in New Zealand, where siliceous (diatom and radiolarian) productivity dominates the early Paleocene and represents a restructured post K-Pg boundary marine algal community (Hollis, 2003; Hollis et al., 2003a, 2003b).

Intriguingly, Zone IV appears to document a return to Zone II algal abundances, with low concentrations of pristane + phytane, low S/(S + H) ratios (Fig. 9B and C), and low ratios of LMW/HMW *n*-alkanes (Fig. 7). This is consistent with multiple changes in productivity regimes in the SW Pacific during the Danian (Taylor et al., 2018).

The evidence for a transient (but evidently mixed and complex) change in marine productivity in Zone II at mid-Waipara River enriches our understanding of distal responses. The S/(S + H) ratios exhibit minimal variation throughout the section, only decreasing from 0.05 to 0.03 in Zone II. Elsewhere at other distal sections, similar muted algal biomarker responses have been observed (Fig. 9D), such as Agost in Spain (Sosa-Montes de Oca et al., 2021), IODP Site 738 (Kerguelen Plateau) and Site 1262 (Walvis Ridge) (Bralower et al., 2020). In contrast, a transient decrease in S/(S + H) ratios in the neritic K-Pg boundary distal section from the Fish Clay in Denmark (Sepúlveda et al., 2009) was observed (Fig. 9D). This could suggest a stronger and more protracted response to the K-Pg impact in the Denmark section than elsewhere. In fact, our S/(S + H) ratios (Fig. 9C) exhibit temporal trends that are markedly similar to those recorded by co-occurring dinoflagellate assemblages (Taylor et al., 2018), with Zones II and IV both characterized by low-productivity, warmer water species (Fig. 9A).

A relatively rapid marine recovery (< 1 Ma) is in general agreement with the 'Living Ocean' model (Coxall et al., 2006; D'Hondt et al., 1998). That model argues that the recovery of the surface-deep water carbon isotope gradient reflects the recovery of the mechanisms for transporting organic matter to depth, rather than a 3 Myr suppression of algal productivity (Adams, 2004; Birch et al., 2016; Coxall et al., 2006; D'Hondt, 2005; D'Hondt et al., 1998). Indeed, the algal biomarker records indicate that marine primary productivity was re-established relatively soon after the K-Pg boundary in the uppermost part of Zone II. It was certainly recovered by Zone III. However, the ongoing biotic change recorded into Zone IV adds nuance to that interpretation and provides an important new perspective on the 'Heterogeneous Ocean' model (Esmeray-Senlet et al., 2015). It appears that the post K-Pg boundary changes in algal productivity reflect not only the direct (but transient) effect of the bolide impact on phytoplankton and the biological pump but longer-term changes in the climatic and oceanographic system.

5.3. Carbon isotopic evidence for post K-Pg boundary changes in the carbon cycle

5.3.1. Bulk organic matter

Negative carbon isotope excursions (-CIEs) in both $\delta^{13}C_{carb}$ and $\delta^{13}C_{TOC}$ are typical in several post-K-Pg boundary intervals (Birch et al., 2016; Sepúlveda et al., 2019). Generally, at those sites, the -CIEs in $\delta^{13}C_{TOC}$ are smaller and shorter than in $\delta^{13}C_{carb}$. However, in the mid-Waipara River section an unexpected +CIE occurs in the $\delta^{13}C_{TOC}$ record (Fig. 10A) but not in *n*-alkanoic acids ($\delta^{13}C_{HMW}$ and $\delta^{13}C_{LMW}$; Fig. 10B and C). This was also observed in the $\delta^{13}C_{TOC}$ record of the Agost distal section (Spain) (Sepúlveda et al., 2019; Sosa-Montes de Oca et al., 2021). We attribute this discrepancy to the complex organic matter source changes across the K-Pg boundary. This could include a transient pulse of reworked ^{13}C-enriched kerogen, similar to what has complicated PETM CIEs (Inglis et al., 2019) or strongly altered terrestrial organic matter as observed in the same section during the Paleocene Carbon Isotope Maximum (or Waipara Event) as documented by Hollis et al. (2022). Although it is unclear what the specific source of ^{13}C-enriched organic matter would have been, the impact of reworked organic matter on the fidelity of the bulk TOC carbon isotopic record has been documented previously (Carmichael et al., 2019). Instead, we examine changes in the carbon cycle recorded by both HMW (higher plant) (Fig. 10B) and LMW (aquatic bacteria and algae) (Fig. 10C) *n*-alkanoic acids.

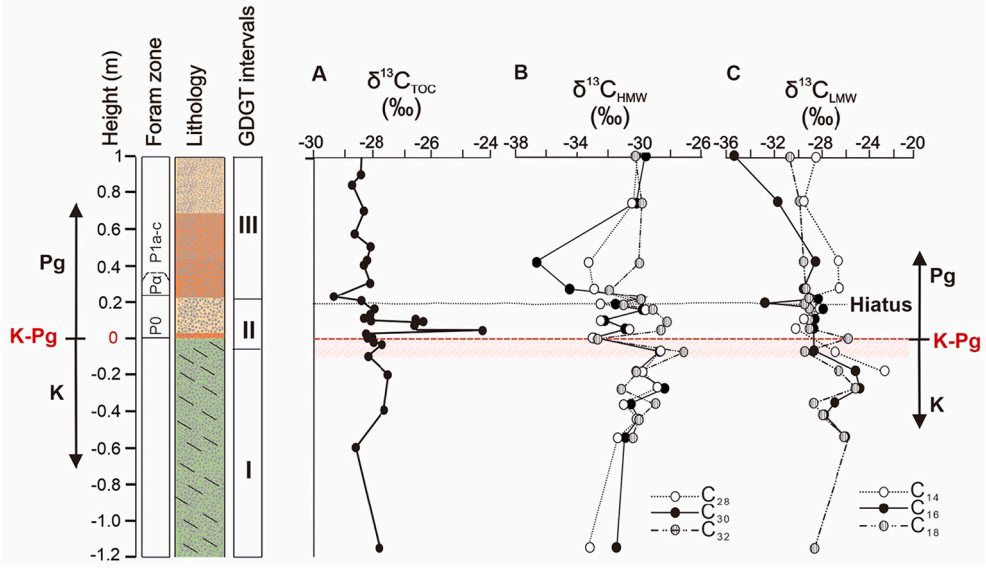

Fig. 10. Carbon Isotopic data at the mid-Waipara River K-Pg section: (A) carbon isotopic compositions of bulk organic carbon ($\delta^{13}C_{TOC}$); (B) carbon isotopic compositions of high molecular weight alkanoic acids ($\delta^{13}C$HMW); and (C) carbon isotopic compositions of low molecular weight alkanoic acids ($\delta^{13}C_{LMW}$).

5.3.2. Higher plant biomarkers

Higher plant $\delta^{13}C$ values are governed by the isotopic composition of substrate carbon, i.e. CO_2 (Arens and Jahren, 2000; Popp et al., 1989), fractionation during carbon assimilation (ε_p) (Farquhar et al., 1982, 1989; Popp et al., 1989) and environmental conditions that influence ε_p values, such as water stress (e.g. Diefendorf et al., 2010, 2011; Kohn, 2010) and CO_2 levels (Cui and Schubert, 2016). Maastrichtian *n*-alkanoic acid $\delta^{13}C_{HMW}$ mean values increase from about −30 ‰ to – 29 ‰ just prior to the K-Pg boundary (Table in supplementary material). A $\delta^{13}C$ C_{29} *n*-alkane record at Caravaca, Spain (Arinobu et al., 1999) also indicates an ~1 ‰ positive shift before the K-Pg; although the estimated timing is later than observed at mid-Waipara, this may be due to age-model uncertainties. A gradual increase in $\delta^{13}C_{TOC}$ values also occurs in the Sugartite coal section in New Mexico, USA (Beerling et al., 2001), although the exact timing for this trend is also not well constrained. The carbon isotopic records of benthic and planktic carbonate also indicate a long-term enrichment in ^{13}C leading up to the K-Pg, particularly in the Pacific benthic records (Alegret and Thomas, 2013; Cramer et al., 2009; Westerhold et al., 2011), in the bulk (pelagic) carbonate carbon isotope record in the South Atlantic (Kroon et al., 2007; Woelders et al., 2017), at the Gubbio section (Italy) (Coccioni et al., 2010; Voigt et al., 2012), the IODP Site U1403 (North Atlantic) and in Zumaia Section (Spain) (Gilabert et al., 2021), although the shift (~1 ‰) occurs over c. 200 kyr, rather than the c. 20 kyr period observed at mid-Waipara. Thus, it is possible that the observed increase in $\delta^{13}C_{HMW}$ values in the latest Maastrichtian provide further evidence for a change in the $\delta^{13}C$ composition of the atmosphere-ocean reservoir.

Similarly, the decrease in mean $\delta^{13}C_{HMW}$ values between the Maastrichtian (Zone I) and the earliest Danian (Zone II) is consistent with previous records and suggests an injection of ^{13}C-depleted organic matter into the atmosphere (Birch et al., 2016). Similar 2‰ negative shifts in inferred terrestrial organic matter have been observed in C_{29} *n*-alkanes at Caravaca, Spain (Arinobu et al., 1999), in bulk organic carbon isotope records from the Raton Basin, USA (Beerling et al., 2001), and in organic carbon isotope records from the York Canyon section (New Mexico), Hauso Flat (Montana), Hell Creek Road, and Pyramid Butte sections (North Dakota), in the Western Interior of the USA (Arens and Jahren, 2000; Schimmelmann and DeNiro, 1984). The putative input of CO_2 from breakdown of the carbonate-rich target rock of the Chicxculub impact would release isotopically heavy CO_2 into the atmosphere (Gardner and Gilmour, 2002; O'Keefe and Ahrens, 1989), and as such a positive excursion would be expected in $\delta^{13}C_{HMW.}$ With the exception of a small ~1 ‰ positive shift in only C_{32} *n*-alkanoic acid (Fig. 10B), the lack of a $\delta^{13}C$ positive excursion in higher plant biomarkers in the mid-Waipara section supports calculations by Arinobu et al., 1999 that suggest a 1.4 ‰ – 2.8 ‰ negative carbon isotope excursion could reflect a geologically instantaneous burning of c. 18–24% of terrestrial above-ground biomass. An increase in CO_2 could also lead to an increase in ε_p and an associated decrease in $\delta^{13}C_{HMW}$ values (Arens and Jahren, 2000; Cui and Schubert, 2016), amplifying the impact of a shift in the carbon isotopic composition of the atmosphere. Other workers, however, interpret changes in atmospheric $\delta^{13}C$ CO_2 as a response to various climatic and eustatic factors (Gröcke et al., 1999; Kaiho et al., 1996).

Intriguingly, these low values extend into Zone III. The hiatus between Zones II and III means that we cannot ascertain the definite trends from c. 23 kyr – 1 myr post K-Pg or draw conclusions about carbon cycle perturbations through that interval. However, if the low $\delta^{13}C_{HMW}$ values at the base of Zone III are representative of the missing strata, they are broadly consistent with records from other terrestrial settings. These include organic matter from continental sections in Montana, Wyoming, North Dakota and New Mexico in the Western Interior of the United States (Arens and Jahren, 2000; Beerling et al., 2001; Maruoka et al., 2007; Schimmelmann and DeNiro, 1984) and China (Clyde et al., 2010) that all document a return to late Cretaceous $\delta^{13}C$ values levels after about 1 myr. Previous observations of terrestrial organic matter and coeval megafloral and microfloral analysis also indicate the persistence of negative $\delta^{13}C$ values through the plant community recovery phases into the relatively well-established restructured assemblages (Beerling et al., 2001). The authors suggest this is evidence that while terrestrial plant communities recovered relatively quickly after the K-Pg boundary event, perturbations in biogeochemical cycling by marine ecosystems continued well after the terrestrial recovery.

5.3.3. Aquatic (Bacterial and Algal) biomarkers

As with higher plant $\delta^{13}C$ values, the $\delta^{13}C$ of marine algae is governed by the isotopic composition of the substrate carbon as well as the magnitude of carbon isotope discrimination during photosynthesis (ε_p). In marine algae, the latter is a function of the isotope fractionations associated with carbon transport and fixation, the concentrations of extra- and intercellular [$CO_{2(aq)}$] (Hayes, 1993; Popp et al., 1989), cell size and volume, nutrient availability and growth rate (Bidigare et al., 1997; Cassar et al., 2002; Rau et al., 1996; Verity et al., 1992). LMW *n*-alkanoic acid $\delta^{13}C$ values ($\delta^{13}C_{LMW}$) are used here to reconstruct marine algal $\delta^{13}C$, assuming an algal (likely mixed) source of these widespread compounds.

The $\delta^{13}C_{LMW}$ record's temporal pattern is similar to that of the $\delta^{13}C_{HMW}$, with a decrease in the latest Cretaceous and low values though Zone II. The deviations from this trend are two outliers, one at the boundary (C_{18} $\delta^{13}C_{LMW}$) and one at the top (C_{16} $\delta^{13}C_{LMW}$), which could reflect unstable productivity/growth rates as suggested for the aftermath of the K-Pg (Hollander et al., 1993), or may be a consequence of the dramatic changes in algal community structure associated with the mass extinction (Zachos et al., 1989) or also mixing of material from above the hiatus.

Despite this variability, we expect the HMW and LMW alkanoic acid $\delta^{13}C$ records to share some features given the connection between marine and atmospheric carbon reservoirs. Indeed, similar to the $\delta^{13}C_{HMW}$ record, $\delta^{13}C_{LMW}$ values decrease in Zone II, and this is consistent with global marine pelagic carbonate records. Negative shifts in $\delta^{13}C$ of a similar magnitude across the K-Pg boundary are recorded in pelagic carbonate elsewhere, e.g. in the South Atlantic ODP Site 1262 (Kroon et al., 2007). Transient ^{13}C-depletion of surface dissolved inorganic carbon of −1.5‰ to −2‰ has also been documented in association with the K-Pg boundary at the global stratotype section in El Kef, Tunisia (Keller et al., 1995; Keller and Lindinger, 1989), and at other marine sections worldwide (i.e., Bralower et al., 2020; D'Hondt et al., 1998; Hsü et al., 1982; Stott and Kennett, 1989; Zachos et al., 1989, 1992; Zachos and Arthur, 1986) based on the carbon isotopic composition of pelagic carbonates. The globally recorded decrease in surface $\delta^{13}C$ is associated with little or no change in deep-water $\delta^{13}C$ (Norris et al., 2001a, 2001b), leading to homogenization of the normally-positive marine surface-to-deep water carbon isotope gradient at the K-Pg boundary. This was originally attributed to a geologically brief cessation of primary productivity in the surface ocean due to the extinction of surface ocean biota (D'Hondt et al., 1998; Hsü et al., 1982; Norris et al., 2001a, 2001b; Zachos and Arthur, 1986), but could instead reflect a reduced biological pump (e.g. 'Living Ocean') (Adams, 2004; Birch et al., 2016; Coxall et al., 2006; D'Hondt, 2005; D'Hondt et al., 1998).

As with the HMW *n*-alkanoic acids, lower $\delta^{13}C_{LMW}$ values persist through Zone II and III (Fig. 10); however, unlike the HMW values, $\delta^{13}C_{LMW}$ values remain low through Zone IV (albeit with considerable variability; Fig. 8). Average $\delta^{13}C_{LMW}$ values are ca −27 ‰ and − 29 ‰ in Zones I and IV, respectively. A similar but slightly smaller magnitude long-term trend is also observed in the pelagic bulk carbonate carbon isotope record in neritic and upper bathyal sections in the western Tethys (El Kef and Aïn Settara sections, Tunisia; the Caravaca section, Spain) and northeastern Atlantic Ocean (the Bidart and Loya section, France and the Kulstirenden and Højerup sections, Denmark) (Sepúlveda et al., 2019). A similar decline in $\delta^{13}C$ values is observed in the benthic carbon isotope records of the Southern Ocean (ODP 690; Alegret et al., 2012; Alegret and Thomas, 2013).

It is intriguing that despite some broad similarities, the algal (LMW *n*-

alkanoic acid) and higher plant (HMW *n*-alkanoic acid) carbon isotopic trends differ in many ways, including in sample-to-sample variation. This likely reflects the complex changes in the aftermath of the K-Pg Boundary, including changes in productivity, climate and biotic assemblages, and we do not interpret all of these differences. Nonetheless, the differences in the long-term algal and higher plant carbon isotopic trends reinforce arguments that biogeochemical perturbations in marine ecosystems persisted longer than those in terrestrial settings (Beerling et al., 2001).

6. Conclusion

Biomarker distributions in the neritic K-Pg mid-Waipara River section, ranging from ~0.1 myr before to ~2 myr after the K-Pg boundary, indicate complex changes in the sources of organic matter (OM) input (marine, terrigenous and reworked petrogenic). Although all three of these inputs of OM are persistent, even across the K-Pg boundary, their relative proportions vary dramatically throughout the section. Zone I, which records the last 0.12 myr from the Upper Cretaceous, consists of a mixed OM input. Zone II, which includes the first 0.02 myr after the K-Pg boundary, records a decrease in especially eukaryotic marine but also terrestrial OM inputs as well as a negative carbon isotope excursion consistent with previous work. Zone III, from 1 to 1.1 myr after K-Pg boundary, records a decrease in the input of reworked petrogenic carbon as well as an increase of marine OM, suggesting that primary productivity has fully recovered at that time. Finally, in Zone IV, from 1.1 to 1.69 myr after the K-Pg boundary, algal biomarker abundances return to Zone II values; terrestrial biomarker distributions are distinct from the rest of the record, consistent with previous work suggesting a long-term reorganisation of vegetation in this region. By developing long-term records, we are able to contextualise changes across the K-Pg boundary. First, the similar changes in algal biomarker assemblages in Zone II immediately above the boundary and Zone IV deposited about 1 myr later suggests that oscillations in SW Pacific upwelling regimes, previously documented by dinoflagellate and GDGT assemblages, had a comparable or even greater impact on algal productivity than the bolide impact at this site. Second, biomarkers of putative algal and higher plant origin both document a negative carbon isotope excursion in the early Danian consistent with release of carbon from either catastrophic vegetation loss and/or a decreased biological pump; the decoupling of those records into Zone III suggests that the marine realm recovered more slowly than terrestrial ecosystems.

Declaration of Competing Interest

There are no known conflicts of interest.

Data availability

Data will be made available on request.

Acknowledgments

We are grateful to Fabienne Marret-Davies (Global and Plantary Changeeditor), and both anonymous reviewers, for their valuable comments and suggestions. We thank the Bristol Node of the Natural Environment Research Council (NERC) Life Sciences Mass Spectrometry Facility for technical assistance with respect to the instrumentation used for organic geochemical analysis. C.S.M.O. acknowledges to Newton International post-doctoral fellowship from Royal Society (project reference NIF\R1\191430) and Marie Curie individual fellowship from the European Commission (project reference 101022128-EPROAMA). KWRT and R.D.P. acknowledge funding from the advanced ERC Grant “The Greenhouse Earth System” (T-GRES, project reference 340923). CJH acknowledges the New Zealand Marsden Fund (Grant GNS703).

Appendix A. Supplementary data

Supplementary data to this article can be found online at https://doi.org/10.1016/j.gloplacha.2022.104025.

References

Adams, J.B., 2004. The Cretaceous-Tertiary extinction: modeling carbon flux and ecological response. Paleoceanography 19, 1–13. https://doi.org/10.1029/2002PA000849.

Alegret, L., Thomas, E., 2013. Benthic foraminifera across the Cretaceous/Paleogene boundary in the southern ocean (ODP Site 690): diversity, food and carbonate saturation. Mar. Micropaleontol. 105, 40–51. https://doi.org/10.1016/j.marmicro.2013.10.003.

Alegret, L., Thomas, E., Lohmann, K.C., 2012. End-Cretaceous marine mass extinction not caused by productivity collapse. Proc. Natl. Acad. Sci. U. S. A. 109, 728–732. https://doi.org/10.1073/pnas.1110601109.

Ali, M.M., Mudge, S.M., 2006. Cluster analysis in lipid biomarker studies: a case of the Clyde Sea. Sains Malaysiana 35, 41–47.

Alvarez, L.W., Alvarez, W., Asaro, F., Michel, H.V., 1980. Extraterrestrial cause for the Cretaceous-Tertiary extinction. Science (80) 208, 1095–1108.

Arens, N.C., Jahren, A.H., 2000. Carbon isotope excursion in atmospheric CO_2 at the Cretaceous-Tertiary boundary: evidence from Terrestrial Sediments. Palaios 15, 314. https://doi.org/10.2307/3515539.

Arinobu, T., Ishiwatari, R., Kaiho, K., Lamolda, M.A., 1999. Spike of pyrosynthetic polycyclic aromatic hydrocarbons associated with an abrupt decrease in δ13C of a terrestrial biomarker at the Cretaceous-Tertiary boundary at Caravaca, Spain. Geology 27, 723–726. https://doi.org/10.1130/0091-7613(1999)027<0723.

Artemieva, N., Morgan, J., 2009. Modeling the formation of the K-Pg boundary layer. Icarus 201, 768–780. https://doi.org/10.1016/j.icarus.2009.01.021.

Beerling, D.J., Lomax Jr., B.H., G.R.U, Nichols, D.J., Pillmore, C.L., Handley, L.L., Scrimgeour, C.M., 2001. Evidence for the recovery of terrestrial ecosystems ahead of marine primary production following a biotic crisis at the Cretaceous–Tertiary boundary. J. Geol. Soc. Lond. 158, 737–740.

Bidigare, R.R., Fluegge, A., Freeman, K.H., Hanson, K.L., Hayes, J.M., Hollander, D., Jasper, J.P., King, L.L., Laws, E.A., Milder, J., Millero, F.J., Pancost, R.D., Popp, B.N., Steinberg, P.A., Wakeham, S.G., 1997. Consistent fractionation of 13C in nature and in the laboratory: growth-rate effects in some haptophyte algae. Glob. Biogeochem. Cycles 11, 279–292.

Birch, H.S., Coxall, H.K., Pearson, P.N., Kroon, D., Schmidt, D.N., 2016. Partial collapse of the marine carbon pump after the Cretaceous-Paleogene boundary. Geology 44, 287–290. https://doi.org/10.1130/G37581.1.

Bourbonniere, R.A., Meyers, P.A., 1996. Sedimentary geolipid records of historical changes in the watersheds and productivities of Lakes Ontario and Erie. Limnol. Oceanogr. 41, 352–359. https://doi.org/10.4319/lo.1996.41.2.0352.

Bralower, T.J., Cosmidis, J., Heaney, P.J., Kump, L.R., Morgan, J.V., Harper, D.T., Lyons, S.L., Freeman, K.H., Grice, K., Wendler, J.E., Zachos, J.C., Artemieva, N., Chen, S.A., Gulick, S.P.S., House, C.H., Jones, H.L., Lowery, C.M., Nims, C., Schaefer, B., Thomas, E., Vajda, V., 2020. Origin of a global carbonate layer deposited in the aftermath of the Cretaceous-Paleogene boundary impact. Earth Planet. Sci. Lett. 548, 116476 https://doi.org/10.1016/j.epsl.2020.116476.

Bray, E.E., Evans, E.D., 1961. Distribution of n-paraffins as a clue to recognition of source beds. Geochim. Cosmochim. Acta 22, 2–15. https://doi.org/10.1016/0016-7037(61)90069-2.

van Breugel, Y., Schouten, S., Tsikos, H., Erba, E., Price, G.D., Damsté, J.S.S., 2007. Synchronous negative carbon isotope shifts in marine and terrestrial biomarkers at the onset of the early Aptian oceanic anoxic event 1a: evidence for the release of 13C-depleted carbon into the atmosphere. Paleoceanography 22, 1–13. https://doi.org/10.1029/2006PA001341.

Brooks, R.R., Strong, C.P., Lee, J., Orth, C.J., Gilmore, J.S., Ryan, D.E., Holzbecher, J., 1986. Stratigraphic occurrences of iridium anomalies at four Cretaceous/Tertiary boundary sites in New Zealand. Geology 14, 727–729.

Calvert, S.E., Pedersen, T.F., 1993. Geochemistry of recent oxic and anoxic marine sediments: implications for the geological record. Mar. Geol. 113, 67–88.

Carmichael, M.J., Pancost, R.D., Lunt, D.J., 2018. Changes in the occurrence of extreme precipitation events at the Paleocene–Eocene thermal maximum. Earth Planet. Sci. Lett. 501, 24–36. https://doi.org/10.1016/j.epsl.2018.08.005.

Carmichael, S.K., Waters, J.A., Königshof, P., Suttner, T.J., Kido, E., 2019. Paleogeography and paleoenvironments of the late Devonian Kellwasser event: a review of its sedimentological and geochemical expression. Glob. Planet. Chang. 183, 102984 https://doi.org/10.1016/j.gloplacha.2019.102984.

Carrie, R.H., Mitchell, L., Black, K.D., 1998. Fatty acids in surface sediment at the Hebridean shelf edge, west of Scotland. Org. Geochem. 29, 1583–1593. https://doi.org/10.1016/S0146-6380(98)00160-0.

Cassar, N., Laws, E.A., Popp, B.N., Bidigare, R.R., 2002. Sources of inorganic carbon for photosynthesis in a strain of Phaeodactylum tricornutum. Am. Soc. Limnol. Oceanogr. Inc. 47, 1192–1197. https://doi.org/10.1002/9783527809080.cataz08945.

Castro, J.M., de Gea, G.A., Quijano, M.L., Aguado, R., Froehner, S., Naafs, B.D.A., Pancost, R.D., 2019. Complex and protracted environmental and ecological perturbations during OAE 1a - evidence from an expanded pelagic section from South Spain (Western Tethys). Glob. Planet. Chang. 183, 103030 https://doi.org/10.1016/j.gloplacha.2019.103030.

Clyde, W.C., Ting, S., Snell, K.E., Bowen, G.J., Tong, Y., Koch, P.L., Li, Q., Wang, Y., 2010. New paleomagnetic and stable-isotope results from the Nanxiong basin, China: Implications for the K/T boundary and the timing of paleocene mammalian turnover. J. Geol. 118, 131–143. https://doi.org/10.1086/649893.

Coccioni, R., Frontalini, F., Bancalà, G., Fornaciari, E., Jovane, L., Sprovieri, M., 2010. The Dan-C2 hyperthermal event at Gubbio (Italy): Global implications, environmental effects, and cause(s). Earth Planet. Sci. Lett. 297, 298–305. https://doi.org/10.1016/j.epsl.2010.06.031.

Coxall, H.K., D'Hondt, S., Zachos, J.C., 2006. Pelagic evolution and environmental recovery after the Cretaceous-Paleogene mass extinction. Geology 34, 297–300. https://doi.org/10.1130/G21702.1.

Cramer, B.S., Toggweiler, J.R., Wright, J.D., Katz, M.E., Miller, K.G., 2009. Ocean overturning since the late cretaceous: inferences from a new benthic foraminiferal isotope compilation. Paleoceanography 24, 1–14. https://doi.org/10.1029/2008PA001683.

Cranwell, P.A., Eglinton, G., Robinson, N., 1987. Lipids of aquatic organisms as potential contributors to lacustrine sediments-II. Org. Geochem. 11, 513–527. https://doi.org/10.1016/0146-6380(87)90007-6.

Cui, Y., Schubert, B.A., 2016. Quantifying uncertainty of past pCO2 determined from changes in C3 plant carbon isotope fractionation. Geochim. Cosmochim. Acta 172, 127–138. https://doi.org/10.1016/j.gca.2015.09.032.

Dean, R.A., Whitehead, E.V., 1961. The occurrence of Phytane in petroleum. Tetrahedron Lett. 21, 768–770.

D'Hondt, S., 2005. Consequences of the Cretaceous/Paleogene mass extinction for marine ecosystems. Annu. Rev. Ecol. Evol. Syst. 36, 295–317. https://doi.org/10.1146/annurev.ecolsys.35.021103.105715.

D'Hondt, S., Donaghay, P., Zachos, J.C., Luttenberg, D., Lindinger, M., 1998. Organic carbon fluxes and ecological recovery from the cretaceous-tertiary mass extinction. Science (80) 282, 276–279.

Diefendorf, A.F., Mueller, K.E., Wing, S.L., Koch, P.L., Freeman, K.H., 2010. Global patterns in leaf 13C discrimination and implications for studies of past and future climate. Proc. Natl. Acad. Sci. U. S. A. 107, 5738–5743. https://doi.org/10.1073/pnas.0910513107.

Diefendorf, A.F., Freeman, K.H., Wing, S.L., Graham, H.V., 2011. Production of n-alkyl lipids in living plants and implications for the geologic past. Geochim. Cosmochim. Acta 75, 7472–7485. https://doi.org/10.1016/j.gca.2011.09.028.

Diefendorf, A.F., Sberna, D.T., Taylor, D.W., 2015. Effect of thermal maturation on plant-derived terpenoids and leaf wax n-alkyl components. Org. Geochem. 89–90, 61–70. https://doi.org/10.1016/j.orggeochem.2015.10.006.

Eglinton, G., Clavin, M., 1967. Certain rocks as much as three billion years old have been found to contain organic compounds. What these compounds are and how they may have originated in living matter is under active study. Sci. Am. 216, 32–43.

Eglinton, G., Hamilton, R.J., 1967. Leaf epicuticular waxes. Science (80) 156. https://doi.org/10.1126/science.156.3780.1322, 1322 LP – 1335.

Eglinton, T.I., Eglinton, G., 2008. Molecular proxies for paleoclimatology. Earth Planet. Sci. Lett. 275, 1–16. https://doi.org/10.1016/j.epsl.2008.07.012.

Esmeray-Senlet, S., Wright, J.D., Olsson, R.K., Miller, K.G., Browning, J.V., Quan, T.M., 2015. The cretaceous/Paleogene mass extinction. Paleoceanography 30, 718–738. https://doi.org/10.1002/2014PA002724.Received.

Farquhar, G.D., O'Leary, M.H., Berry, J.A., 1982. On the relationship between carbon isotope discrimination and the intercellular carbon dioxide concentration in leaves. Funct. Plant Biol. 9, 121–137.

Farquhar, G.D., Ehleringer, J.R., Hubick, K.T., 1989. Carbon Isotope Discrimination and Photosynthesis. Annu. Rev. Plant Physiol. Plant Mol. Biol. 40, 503–537. https://doi.org/10.1146/annurev.pp.40.060189.002443.

Gardner, A.F., Gilmour, I., 2002. Organic geochemical investigation of terrestrial Cretaceous-Tertiary boundary successions from Brownie Butte, Montana, and the Raton Basin, New Mexico. Spec. Pap. - Geol. Soc. Am. 356, 351–362.

Gelpi, E., Schneider, H., Mann, J., Oró, J., 1970. Hydrocarbons of geochemical significance in microscopic algae. Phytochemistry 9 (3), 603–612. https://doi.org/10.1016/S0031-9422(00)85700-3. ISSN 0031-9422.

Gilabert, V., Batenburg, S.J., Arenillas, I., Arz, J.A., 2021. Contribution of orbital forcing and Deccan volcanism to global climatic and biotic changes across the Cretaceous-Paleogene boundary at Zumaia, Spain. Geology 49, 1–5. https://doi.org/10.1130/G49214.1/5393375/g49214.pdf.

Gillan, F.T., Hogg, R.W., Drew, E.A., 1984. The sterol and fatty acid compositions of seven tropical seagrasses from North Queensland, Australia. Phytochemistry 23, 2817–2821. https://doi.org/10.1016/0031-9422(84)83021-6.

Gröcke, D.R., Hesselbo, S.P., Jenkyns, H.C., 1999. Carbon-isotope composition of lower cretaceous fossil wood: ocean-atmosphere chemistry and relation to sea-level change. Geology 27, 155–158. https://doi.org/10.1130/0091-7613(1999)027<0155:CICOLC>2.3.CO;2.

Gulick, S.P.S., Bralower, T.J., Ormö, J., Hall, B., Grice, K., Schaefer, B., Lyons, S., Freeman, K.H., Morgan, J.V., Artemieva, N., Kaskes, P., De Graaff, S.J., Whalen, M. T., Collins, G.S., Tikoo, S.M., Verhagen, C., Christeson, G.L., Claeys, P., Coolen, M.J. L., Goderis, S., Goto, K., Grieve, R.A.F., McCall, N., Osinski, G.R., Rae, A.S.P., Riller, U., Smit, J., Vajda, V., Wittmann, A., 2019. The first day of the Cenozoic. Proc. Natl. Acad. Sci. U. S. A. 116, 19342–19351. https://doi.org/10.1073/pnas.1909479116.

Hackley, P.C., Zhang, T., Jubb, A.M., Valentine, B.J., Dulong, F.T., Hatcherian, J.J., 2020. Organic petrography of Leonardian (Wolfcamp a) mudrocks and carbonates, Midland Basin, Texas: the fate of oil-prone sedimentary organic matter in the oil window. Mar. Pet. Geol. 112, 104086 https://doi.org/10.1016/j.marpetgeo.2019.104086.

Handley, L., Talbot, H.M., Cooke, M.P., Anderson, K.E., Wagner, T., 2010. Bacteriohopanepolyols as tracers for continental and marine organic matter supply and phases of enhanced nitrogen cycling on the late Quaternary Congo deep sea fan. Org. Geochem. 41, 910–914. https://doi.org/10.1016/j.orggeochem.2010.04.016.

Hayes, J.M., 1993. Factors controlling 13C contents of sedimentary organic compounds: principles and evidence. Mar. Geol. 113, 111–125.

Hollander, D.J., McKenzie, J.A., Hsü, K.J., 1993. Carbon isotope evidence for unusual plankton blooms and fluctuations of surface water CO2 in "Strangelove Ocean" after terminal cretaceous event. Palaeogeogr. Palaeoclimatol. Palaeoecol. 104, 229–237. https://doi.org/10.1016/0031-0182(93)90134-5.

Hollis, C.J., 2003. The cretaceous/Tertiary boundary event in New Zealand: Profiling mass extinction. New Zeal. J. Geol. Geophys. 46, 307–321. https://doi.org/10.1080/00288306.2003.9515011.

Hollis, C.J., Strong, C.P., 2003. Biostratigraphic review of the Cretaceous/Tertiary boundary transition, mid-Waipara River section, North Canterbury, New Zealand. New Zeal. J. Geol. Geophys. 46, 243–253. https://doi.org/10.1080/00288306.2003.9515007.

Hollis, C.J., Rodgers, K.A., Strong, C.P., Field, B.D., Rogers, K.M., 2003a. Paleoenvironmental changes across the cretaceous/Tertiary boundary in the northern Clarence valley, southeastern Marlborough, New Zealand. New Zeal. J. Geol. Geophys. 46, 209–234. https://doi.org/10.1080/00288306.2003.9515005.

Hollis, C.J., Strong, C.P., Rodgers, K.A., Rogers, K.M., 2003b. Paleoenvironmental changes across the Cretaceous/Tertiary boundary at Flaxbourne River and Woodside Creek, eastern Marlborough, New Zealand. New Zeal. J. Geol. Geophys. 46, 177–197. https://doi.org/10.1080/00288306.2003.9515003.

Hollis, C.J., Naeher, S., Clowes, C.D., Dahl, J., Li, X., Naafs, B.D.A., Pancost, R.D., Taylor, K.W.R., Ventura, G.T., Sykes, R., 2022. Late Paleocene CO_2 drawdown, climatic cooling, and terrestrial denudation in the Southwest Pacific. Clim. Past Discuss. 1–32. https://doi.org/10.5194/cp-2021-122.

Hopmans, E.C., Weijers, J.W.H., Schefuß, E., Herfort, L., Sinninghe Damsté, J.S., Schouten, S., 2004. A novel proxy for terrestrial organic matter in sediments based on branched and isoprenoid tetraether lipids. Earth Planet. Sci. Lett. 224, 107–116. https://doi.org/10.1016/j.epsl.2004.05.012.

Hsü, K.J., McKenzie, J.A., 1985. A "Strangelove" Ocean in the Earliest Tertiary. Carbon Cycle Atmos (CO Nat. Var. Archean to Present 487–492).

Hsü, K.J., He, Q., McKenzie, J.A., Weissert, H., Perch-Nielsen, K., Oberhänsli, H., Kelts, K., LaBrecque, J., Tauxe, L., Krähenbühl, U., 1982. Mass mortality and its environmental and evolutionary consequences. Science (80) 216, 249–256.

Huang, W.Y., Meinschew, W.G., 1979. Sterols as ecological indicators. Geochim. Cosmochim. Acta 43, 739–745.

Hull, P.M., Bornemann, A., Penman, D.E., Henehan, M.J., Norris, R.D., Wilson, P., Blum, P., Alegret, L., Batenburg, S.J., Bown, P.R., Bralower, T.J., Cournede, C., Deutsch, A., Donner, B., Friedrich, O., Jehle, S., Kim, H., Kroon, D., Lippert, P.C., Loroch, D., Moebius, I., Moriya, K., Peppe, D.J., Ravizza, G.E., Röhl, U., Schueth, J. D., Sepúlveda, J., Sexton, P.F., Sibert, E.C., Summons, R.E., Thomas, E., Westerhold, T., Whiteside, J.H., Yamaguchi, T., Zachos, J.C., 2020. On impact and volcanism across the Cretaceous-Paleogene boundary. Science (80) 367, 266–272.

Inglis, G.N., Farnsworth, A., Collinson, M.E., Carmichael, M.J., Naafs, B.D.A., Lunt, D.J., Valdes, P.J., Pancost, R.D., 2019. Terrestrial environmental change across the onset of the PETM and the associated impact on biomarker proxies: a cautionary tale. Glob. Planet. Chang. 181, 102991 https://doi.org/10.1016/j.gloplacha.2019.102991.

Ivany, L.C., Salawitch, R.J., 1993. Carbon isotopic evidence for biomass burning at the K-T boundary. Geology 21, 487–490.

Jones, D.M., Carter, J.F., Eglinton, G., Jumeau, E.J., Fenwick, C.S., 1991. Determination of δ ^{13}C values of sedimentary straight chain and cyclic alcohols by gas chromatography/isotope ratio mass spectrometry. Biol. Mass Spectrom. 20, 641–646.

Kaiho, K., Arinobu, T., Ishiwatari, R., Morgans, H.E.G., Okada, H., Takeda, N., Tazaki, K., Zhou, G., Kajiwara, Y., Matsumoto, R., Hirai, A., Niitsuma, N., Wada, H., 1996. Lasted Paleocene benthic foraminiferal extinction and environmental changes at Tawanui, New Zealand. Paleoceanography 11, 447–465.

Keller, G., Lindinger, M., 1989. Stable isotope, TOC and CaCO3 record across the cretaceous/tertiary boundary at El Kef, Tunisia. Palaeogeogr. Palaeoclimatol. Palaeoecol. 73, 243–265. https://doi.org/10.1016/0031-0182(89)90007-2.

Keller, G., Li, L., MacLeod, N., 1995. The Cretaceous/Tertiary boundary stratotype section at El Kef, Tunisia: how catastrophic was the mass extinction? Palaeogeogr. Palaeoclimatol. Palaeoecol. 119, 221–254. https://doi.org/10.1016/0031-0182(95)00009-7.

Kohn, M.J., 2010. Carbon isotope compositions of terrestrial C3 plants as indicators of (paleo)ecology and (paleo)climate. Proc. Natl. Acad. Sci. U. S. A. 107, 19691–19695. https://doi.org/10.1073/pnas.1004933107.

Kring, D.A., 2007. The Chicxulub impact event and its environmental consequences at the Cretaceous-Tertiary boundary. Palaeogeogr. Palaeoclimatol. Palaeoecol. 255, 4–21. https://doi.org/10.1016/j.palaeo.2007.02.037.

Kroon, D., Zachos, J.C., Party, L., 2007. Leg 208 synthesis: Cenozoic climate cycles and excursions. Proc. Ocean Drill. Program Sci. Results 208, 1–55. doi: https://doi.org/10.2973/odp.proc.sr.208.201.2007.

Kvenvolden, K.A., 1967. Normal fatty acids in sediments. J. Am. Oil Chem. Soc. 44, 628–636. https://doi.org/10.1007/BF02680031.

Lowery, C.M., Bralower, T.J., Owens, J.D., Rodríguez-Tovar, F.J., Jones, H., Smit, J., Gulick, S., Joanna, V., Green, S., Chenot, E., Whalen, M.T., Claeys, P., Farley, K., Sean, P., 2018. Rapid recovery of life at ground zero of the end-Cretaceous mass extinction. Nature. https://doi.org/10.1038/s41586-018-0163-6.

Lowery, C.M., Bown, P.R., Fraass, A.J., Hull, P.M., 2020. Ecological response of plankton to environmental change: thresholds for extinction Christopher. Annu. Rev. Earth Planet. Sci. 48 https://doi.org/10.1146/annurev-earth-081619-052818, 16.1–16.27.

Lyle, M., 1988. Climatically forced organic carbon burial in equatorial Atlantic and Pacific Oceans. Nature 335, 55–56.
Lyons, S.L., Karp, A.T., Bralower, T.J., Grice, K., Schaefer, B., Gulick, S.P.S., Morgan, J. V., Freeman, K.H., 2020. Organic matter from the Chicxulub crater exacerbated the K-Pg impact winter. Proc. Natl. Acad. Sci. U. S. A. 117, 25327–25334. https://doi.org/10.1073/pnas.2004596117.
Mackenzie, A.S., Patience, R.L., Maxwell, J.R., Vandenbroucke, M., Durand, B., 1980. Molecular parameters of maturation in the Toarcian shales, Paris Basin, France—I. changes in the configurations of acyclic isoprenoid alkanes, steranes and triterpanes. Geochim. Cosmochim. Acta 44, 1709–1721. https://doi.org/10.1016/0016-7037(80)90222-7.
Maruoka, T., Koeberl, C., Bohor, B.F., 2007. Carbon isotopic compositions of organic matter across continental Cretaceous-Tertiary (K-T) boundary sections: Implications for paleoenvironment after the K-T impact event. Earth Planet. Sci. Lett. 253, 226–238. https://doi.org/10.1016/j.epsl.2006.10.028.
Meyers, P.A., 1997. Organic geochemical proxies of paleoceanographic, paleolimnologic, and paleoclimatic processes. Org. Geochem. 27, 213–250. https://doi.org/10.1016/S0146-6380(97)00049-1.
Milligan, J.N., Flynn, A.G., Kowalczyk, J.B., Barclay, R.S., Geng, J., Royer, D.L., Peppe, D.J., 2022. Moderate to elevated atmospheric CO 2 during the early Paleocene Recorded by Platanites Leaves of the San Juan Basin, New Mexico. Paleoceanogr. Paleoclimatol 37, 1–12. https://doi.org/10.1029/2021pa004408.
Moldowan, J. Michael, Seifert, W.K., Gallegos, E.J., 1985b. Relationship between petroleum composition and depositional environment of petroleum source rocks1. Am. Assoc. Pet. Geol. Bull. 69, 1255–1268. https://doi.org/10.1306/AD462BC8-16F7-11D7-8645000102C1865D.
Moldowan, J.M., Seifert, W.K., Gallegos, E.J., 1985a. Relationship between petroleum composition and depositional environment of petroleum source rocks. Am. Assoc. Pet. Geol. Bull. 69, 1255–1268. https://doi.org/10.1306/ad462bc8-16f7-11d7-8645000102c1865d.
Norris, R.D., Klaus, A., Kroon, D., 2001a. Mid-Eocene deep water, the late Palaeocene thermal maximum and continental slope mass wasting during the cretaceous-palaeogene impact. Geol. Soc. Spec. Publ. 183, 23–48. https://doi.org/10.1144/GSL.SP.2001.183.01.02.
Norris, R.D., Kroon, D., Huber, B.T., Erbacher, J., 2001b. Cretaceous-Palaeogene Ocean and climate change in the subtropical North Atlantic. Geol. Soc. Spec. Publ. 183, 1–22. https://doi.org/10.1144/GSL.SP.2001.183.01.01.
O'Keefe, J.D., Ahrens, T.J., 1989. Impact production of CO2 by the cretaceous/Tertiary extinction bolide and the resultant heating of the Earth. Nature 338, 247–249. https://doi.org/10.1038/338247a0.
Ourisson, G., Albrecht, P., Rohmer, M., 1979. The Hopanoids: palaeochemistry and biochemistry of a group of natural products. Pure Appl. Chem. 51, 709–729. https://doi.org/10.1351/pac197951040709.
Pälike, H., 2013. Impact and Extinction. Science (80) 339, 655–656.
Pancost, R.D., Boot, C.S., 2004. The palaeoclimatic utility of terrestrial biomarkers in marine sediments. Mar. Chem. 92, 239–261. https://doi.org/10.1016/j.marchem.2004.06.029.
Pancost, R.D., Baas, M., Van Geel, B., Sinninghe Damsté, J.S., 2002. Biomarkers as proxies for plant inputs to peats: an example from a sub-boreal ombrotrophic bog. Org. Geochem. 33, 675–690. https://doi.org/10.1016/S0146-6380(02)00048-7.
Pancost, R.D., Taylor, K.W.R., Inglis, G.N., Kennedy, E.M., Handley, L., Hollis, C.J., Crouch, E.M., Pross, J., Huber, M., Schouten, S., Pearson, P.N., Morgans, H.E.G., Raine, J.I., 2013. Early Paleogene evolution of terrestrial climate in the SW Pacific, Southern New Zealand. Geochem. Geophys. Geosyst. 14, 5413–5429. https://doi.org/10.1002/2013GC004935.
Peters, K.E., Moldowan, J.M., 1991. Effects of source, thermal maturity, and biodegradation on the distribution and isomerization of homohopanes in petroleum. Org. Geochem. 17, 47–61. https://doi.org/10.1016/0146-6380(91)90039-M.
Peters, K.E., Peters, K.E., Walters, C.C., Moldowan, J.M., 2005. The Biomarker Guide. Cambridge University Press.
Popp, B.N., Takigiku, R., Hayes, J.M., Louda, J.W., Baker, E.W., 1989. The post-Paleozoic chronology and mechanism of 13C depletion in primary marine organic matter. Am. J. Sci. 289, 436–454. https://doi.org/10.2475/ajs.289.4.436.
Poynter, J., Eglinton, G., 1990. Molecular composition of three sediments from hole 717C: the Bengal Fan. Proc. Sci. Results 116, 155–161. https://doi.org/10.2973/odp.proc.sr.116.151.1990 (ODP, Leg 116, distal Bengal Fan).
Rau, G.H., Riebesell, U., Wolf-Gladrow, D., 1996. A model of photosynthetic 13C fractionation by marine phytoplankton based on diffusive molecular CO2 uptake. Mar. Ecol. Prog. Ser. 133, 275–285. https://doi.org/10.3354/meps133275.
Renne, P.R., Sprain, C.J., Richards, M.A., Self, S., Vanderkluysen, L., Pande, K., 2015. Possibly induced by impact. Science (80) 350, 76–78. https://doi.org/10.1126/science.aac7549.
Rieley, G., Collier, R.J., Jones, D.M., Eglinton, G., Eakint, P.A., Fallickt, A.E., 1991. Sources of sedimentary lipids deduced from stable carbon- isotope analyses of individual compounds. Nature 352, 425–427.
Rodríguez-Tovar, F.J., Lowery, C.M., Bralower, T.J., Gulick, S.P.S., Jones, H.L., 2020. Rapid macrobenthic diversification and stabilization after the end-cretaceous mass extinction event. Geology 48, 1048–1052. https://doi.org/10.1130/g47589.1.
Rontani, J.F., Volkman, J.K., 2003. Phytol degradation products as biogeochemical tracers in aquatic environments. Org. Geochem. 34, 1–35.
Scalan, R.S., Smith, J.E., 1970. An improved measure of the odd-even predominance in the normal alkanes of sediment extracta and petroleum. Geochim. Cosmochim. Acta 34, 611–620.
Schaefer, B., Grice, K., Coolen, M.J.L., Summons, R.E., Cui, X.X., Bauersachs, T., Schwark, L., Böttcher, M.E., Bralower, T.J., Lyons, S.L., Freeman, K.H., Cockell, C.S., Gulick, S.S., Morgan, J.V., Whalen, M.T., Lowery, C.M., Vajda, V., 2020. Microbial life in the nascent chicxulub crater. Geology 48, 1–5. https://doi.org/10.3997/2214-4609.201902850.
Schefuß, E., Ratmeyer, V., Stuut, J.B.W., Jansen, J.H.F., Sinninghe Damsté, J.S., 2003. Carbon isotope analyses of n-alkanes in dust from the lower atmosphere over the central eastern Atlantic. Geochim. Cosmochim. Acta 67, 1757–1767. https://doi.org/10.1016/S0016-7037(02)01414-X.
Schimmelmann, A., DeNiro, M.J., 1984. Elemental and stable isotope variations of organic matter from a terrestrial sequence containing the Cretaceous/Tertiary boundary at York Canyon, New Mexico. Earth Planet. Sci. Lett. 68, 392–398. https://doi.org/10.1016/0012-821X(84)90124-9.
Schoene, B., Samperton, K.M., Eddy, M.P., Keller, G., Adatte, T., Bowring, S.A., Khadri, S. F.R., Gertsch, B., 2015. U-Pb geochronology of the Deccan Traps and relation to the end-cretaceous mass extinction. Science (80) 347, 182–184. https://doi.org/10.1126/science.aaa0118.
Schoene, B., Eddy, M.P., Samperton, K.M., Keller, C.B., Keller, G., Adatte, T., Khadri, S.F. R., 2019. U-Pb constraints on pulsed eruption of the Deccan Traps across the end-cretaceous mass extinction. Science (80) 363, 862–866. https://doi.org/10.1126/science.aau2422.
Schouten, S., Ossebaar, J., Brummer, G.J., Elderfield, H., Sinninghe Damsté, J.S., 2007. Transport of terrestrial organic matter to the deep North Atlantic Ocean by ice rafting. Org. Geochem. 38, 1161–1168. https://doi.org/10.1016/j.orggeochem.2007.02.012.
Schouten, S., Pitcher, A., Hopmans, E.C., Villanueva, L., van Bleijswijk, J., Sinninghe Damsté, J.S., 2012. Intact polar and core glycerol dibiphytanyl glycerol tetraether lipids in the Arabian Sea oxygen minimum zone: I. Selective preservation and degradation in the water column and consequences for the TEX86. Geochim. Cosmochim. Acta 98, 228–243. https://doi.org/10.1016/j.gca.2012.05.002.
Schulte, P., Alegret, L., Arenillas, I., Arz, J.A., Barton, P.J., Bown, P.R., Bralower, T.J., Christeson, G.L., Claeys, P., Cockell, C.S., Collins, G.S., Deutsch, A., Goldin, T.J., Goto, K., Grajales-Nishimura, J.M., Grieve, R.A.F., Gulick, S.P.S., Johnson, K.R., Kiessling, W., Koeberl, C., Kring, D.A., MacLeod, K.G., Matsui, T., Melosh, J., Montanari, A., Morgan, J.V., Neal, C.R., Nichols, D.J., Norris, R.D., Pierazzo, E., Ravizza, G., Rebolledo-Vieyra, M., Reimold, W.U., Robin, E., Salge, T., Speijer, R.P., Sweet, A.R., Urrutia-Fucugauchi, J., Vajda, V., Whalen, M.T., Willumsen, P.S., 2010. The chicxulub asteroid impact and mass extinction at the cretaceous-paleogene boundary. Science (80) 327, 1214–1218. https://doi.org/10.1126/science.1177265.
Schwark, L., Empt, P., 2006. Sterane biomarkers as indicators of palaeozoic algal evolution and extinction events. Palaeogeogr. Palaeoclimatol. Palaeoecol. 240, 225–236. https://doi.org/10.1016/j.palaeo.2006.03.050.
Seifert, W.K., Moldowan, J.M., 1980. The effect of thermal stress on source-rock quality as measured by hopane stereochemistry. Phys. Chem. Earth 12, 229–237. https://doi.org/10.1016/0079-1946(79)90107-1.
Sepúlveda, J., Wendler, J.E., Summons, R.E., Hinrichs, K.-U., 2009. Rapid resurgence of marine productivity after the Cretaceous-Paleogene mass extinction. Science (80) 326, 129–132. https://doi.org/10.1126/science.1176233.
Sepúlveda, J., Alegret, L., Thomas, E., Haddad, E., Cao, C., Summons, R.E., 2019. Stable isotope constraints on marine productivity across the Cretaceous-Paleogene mass extinction. Paleoceanogr. Paleoclimatol. 34, 1195–1217. https://doi.org/10.1029/2018PA003442.
Smit, J., 1999. The global stratigraphy of the Cretaceous-Tertiary boundary impact ejecta. Annu. Rev. Earth Planet. Sci. 27, 75–113.
Sosa-Montes de Oca, C., Martínez-Ruiz, F., Rodríguez-Tovar, F.J., 2013. Bottom-water conditions in a marine basin after the Cretaceous-Paleogene impact event: timing the recovery of oxygen levels and productivity. PLoS One 8, e82242. https://doi.org/10.1371/journal.pone.0082242.
Sosa-Montes de Oca, C., de Lange, G.J., Martínez-Ruiz, F., Rodríguez-Tovar, F.J., 2018. Application of laser ablation-ICP-MS to determine high-resolution elemental profiles across the Cretaceous/Paleogene boundary at Agost (Spain). Palaeogeogr. Palaeoclimatol. Palaeoecol. 497, 128–138. https://doi.org/10.1016/j.palaeo.2018.02.012.
Sosa-Montes de Oca, C., de Lange, G.J., Martínez-Ruiz, F., Ortega-Huertas, M., Rodríguez-Tovar, F.J., 2020. Microscale trace-element distribution across the cretaceous/Palaeogene ejecta layer at the Agost section: Constraining the recovery of pre-impact conditions. Chem. Geol. 533 https://doi.org/10.1016/j.chemgeo.2019.119431.
Sosa-Montes de Oca, C., Rodrigo-Gámiz, M., Martínez-Ruiz, F., Rodríguez-Tovar, F.J., Castro, J.M., Quijano, M.L., Pancost, R.D., 2021. Minor changes in biomarker assemblages in the aftermath of the Cretaceous-Paleogene mass extinction event at the Agost distal section (Spain). Palaeogeogr. Palaeoclimatol. Palaeoecol. 569, 110310 https://doi.org/10.1016/j.palaeo.2021.110310.
Stott, L.D., Kennett, J.P., 1989. New constraints on early Tertiary palaeoproductivity from carbon isotopes in foraminifera. Nature 342, 526.
Strong, C.P., 1984. Cretaceous—tertiary boundary, mid-waipara river section, North Canterbury, New Zealand. New Zeal. J. Geol. Geophys. 27, 231–234. https://doi.org/10.1080/00288306.1984.10422531.
Taylor, K.W.R., Huber, M., Hollis, C.J., Hernandez-Sanchez, M.T., Pancost, R.D., 2013. Re-evaluating modern and Palaeogene GDGT distributions: implications for SST reconstructions. Glob. Planet. Chang. 108, 158–174. https://doi.org/10.1016/j.gloplacha.2013.06.011.
Taylor, K.W.R., Willumsen, P.S., Hollis, C.J., Pancost, R.D., 2018. South Pacific evidence for the long-term climate impact of the cretaceous/Paleogene boundary event. Earth-Sci. Rev. 179, 287–302. https://doi.org/10.1016/j.earscirev.2018.02.012.
Toon, O.B., Zahnle, K., Morrison, D., Turco, R.P., Covey, C., 1997. Environmental perturbations caused by the impacts of asteroids and comets. Ann. N. Y. Acad. Sci. 822, 401–402. https://doi.org/10.1111/j.1749-6632.1997.tb48357.x.

Tschudy, R.H., Pillmore, C.L., Orth, C.J., Gilmore, J.S., Knight, J.D., 1984. Disruption of the terrestrial plant ecosystem at the Cretaceous-Tertiary boundary, Western Interior. Science (80) 225, 1030–1032.

Vajda, V., Raine, J.I., 2003b. Pollen and spores in marine Cretaceous/Tertiary boundary sediments at mid-Waipara River, North Canterbury, New Zealand. New Zeal. J. Geol. Geophys. 46, 255–273. https://doi.org/10.1080/00288306.2003.9515008.

Vajda, V., Raine, J.I., Hollis, C.J., 2001. Indication of global deforestation at the Cretaceous-Tertiary boundary by New Zealand fern spike. Science (80) 294, 1700–1702. https://doi.org/10.1126/science.1064706.

Vajda, Vivi, Raine, J.I., 2003a. Pollen and spores in marine Cretaceous/Tertiary boundary sediments at mid-Waipara River, North Canterbury, New Zealand. New Zeal. J. Geol. Geophys. 46, 255–273. https://doi.org/10.1080/00288306.2003.9515008.

Vellekoop, J., Woelders, L., Açikalin, S., Smit, J., Van De Schootbrugge, B., Yilmaz, I.O., Brinkhuis, H., Speijer, R.P., 2017. Ecological response to collapse of the biological pump following the mass extinction at the Cretaceous-Paleogene boundary. Biogeosciences 14, 885–900. https://doi.org/10.5194/bg-14-885-2017.

Verity, P.G., Robertson, C.Y., Tronzo, C.R., Andrews, M.G., Nelson, J.R., Sieracki, M.E., 1992. Relationships between cell volume and the carbon and nitrogen content of marine photosynthetic nanoplankton. Limnol. Oceanogr. 37, 1434–1446. https://doi.org/10.4319/lo.1992.37.7.1434.

Versteegh, G.J.M., Schefuß, E., Dupont, L., Marret, F., Sinninghe Damsté, J.S., Jansen, J. H.F., 2004. Taraxerol and Rhizophora pollen as proxies for tracking past mangrove ecosystems. Geochim. Cosmochim. Acta 68, 411–422. https://doi.org/10.1016/S0016-7037(03)00456-3.

Voigt, S., Gale, A.S., Jung, C., Jenkyns, H.C., 2012. Global correlation of Upper Campanian-Maastrichtian successions using carbon-isotope stratigraphy: develoment of a new Maastrichtian timescale. Newsl. Stratigr. 45, 25–53.

Wannigama, G.P., Volkman, J.K., Gillan, F.T., Nichols, P.D., Johns, R.B., 1981. A comparison of lipid components of the fresh and dead leaves and pneumatophores of the mangrove Avicennia marina. Phytochemistry 20, 659–666.

Weijers, J.W.H., Schouten, S., Spaargaren, O.C., Sinninghe Damsté, J.S., 2006. Occurrence and distribution of tetraether membrane lipids in soils: Implications for the use of the TEX86 proxy and the BIT index. Org. Geochem. 37, 1680–1693. https://doi.org/10.1016/j.orggeochem.2006.07.018.

Westerhold, T., Rhl, U., Donner, B., McCarren, H.K., Zachos, J.C., 2011. A complete high-resolution Paleocene benthic stable isotope record for the Central Pacific (ODP Site 1209). Paleoceanography 26, 1–13. https://doi.org/10.1029/2010PA002092.

Willumsen, P.S., 2000. Late cretaceous to early Paleocene palynological changes in midlatitude Southern Hemisphere, New Zealand. GFF 122, 180–181.

Willumsen, P.S., 2006. Palynodinium minus sp. nov., a new dinoflagellate cyst from the Cretaceous-Paleogene transition in New Zealand; its significance and palaeoecology. Cretac. Res. 27, 954–963. https://doi.org/10.1016/j.cretres.2006.06.002.

Woelders, L., Vellekoop, J., Kroon, D., Smit, J., Casadío, S., Prámparo, M.B., Dinarès-Turell, J., Peterse, F., Sluijs, A., Lenaerts, J.T.M., Speijer, R.P., 2017. Latest cretaceous climatic and environmental change in the South Atlantic region. Paleoceanography 32, 466–483. https://doi.org/10.1002/2016PA003007.

Wolbach, W.S., Anders, E., Orth, C.J., Brooks, R.R., 1988. Global fire at the Cretaceous-Tertiary boundary Wendy. Nature 334, 665–669.

Wolfe, J.A., Upchurch, G.R., 1987. Leaf assemblages across the Cretaceous-Tertiary boundary in the Raton Basin, New Mexico and Colorado. Proc. Natl. Acad. Sci. 84, 5096–5100. https://doi.org/10.1073/pnas.84.15.5096.

Xie, S., Pancost, R.D., Wang, Y., Yang, H., Wignall, P.B., Luo, G., Jia, C., Chen, L., 2010. Cyanobacterial blooms tied to volcanism during the 5 m.y. Permo-Triassic biotic crisis. Geology 38, 447–450. https://doi.org/10.1130/G30769.1.

Zachos, J.C., Arthur, M.A., 1986. Paleoceanography of the Cretaceous/Tertiary boundary event: Inferences from stable isotopic and other data. Paleoceanography 1, 5–26.

Zachos, J.C., Arthur, M.A., Dean, W.E., 1989. Geochemical evidence for suppression of pelagic marine productivity at the Cretaceous/Tertiary boundary. Nature 337, 61–64. https://doi.org/10.1038/337061a0.

Zachos, J.C., Aubry, M.P., Berggren, W.A., Ehrendorfer, T., Heider, F., Lohmann, K.C., 1992. Chemobiostratigraphy of the cretaceous/Paleocene boundary at Site 750, southern Kerguelen Plateau. Proc. Sci. Results 120, 961–977. https://doi.org/10.2973/odp.proc.sr.120.188.1992 (ODP, Leg 120 Cent. Kerguelen Plateau).